HHS Public Access

Author manuscript

Acta Biomater. Author manuscript; available in PMC 2022 October 15.

Published in final edited form as:

Acta Biomater. 2021 October 15; 134: 144–159. doi:10.1016/j.actbio.2021.06.034.

Tissue engineered bovine saphenous vein extracellular matrix scaffolds produced via antigen removal achieve high *in vivo* patency rates

Manuela Lopera Higuita[a], **Juan F. Lopera Giraldo**[b], **Tiffany L. Sarrafian**[c], **Leigh G. Griffiths**[d,*]

[a]Department of Radiology, Mayo Clinic, 200 1st St SW, Rochester, MN 55905, USA

[b]Department of Plastic Surgery, Clínica Las Américas, Antioquia, Dg. 75B ##2A-80/140, Medellín, Colombia

[c]Department of Thoracic Surgery, Mayo Clinic, 200 1st St SW, Rochester MN, USA

[d]Department of Cardiovascular Diseases, Mayo Clinic, 200 1st St SW, Rochester, MN 55905, USA

Abstract

Diseases of small diameter blood vessels encompass the largest portion of cardiovascular diseases, with over 4.2 million people undergoing autologous vascular grafting every year. However, approximately one third of patients are ineligible for autologous vascular grafting due to lack of suitable donor vasculature. Acellular extracellular matrix (ECM) scaffolds derived from xenogeneic vascular tissue have potential to serve as ideal biomaterials for production of off-the-shelf vascular grafts capable of eliminating the need for autologous vessel harvest. A modified antigen removal (AR) tissue process, employing aminosulfabetaine-16 (ASB-16) was used to create off-the-shelf small diameter (< 3 mm) vascular graft from bovine saphenous vein ECM scaffolds with significantly reduced antigenic content, while retaining native vascular ECM protein structure and function. Elimination of native tissue antigen content conferred graft-specific adaptive immune avoidance, while retention of native ECM protein macromolecular structure resulted in pro-regenerative cellular infiltration, ECM turnover and innate immune self-recognition in a rabbit subpannicular model. Finally, retention of the delicate vascular basement membrane protein integrity conferred endothelial cell repopulation and 100% patency rate in a rabbit jugular interposition model, comparable only to Autograft implants. Alternatively, the lack of these important basement membrane proteins in otherwise identical scaffolds yielded a patency rate of only 20%. We conclude that acellular antigen removed bovine saphenous vein ECM scaffolds have potential to serve as ideal off-the-shelf small diameter vascular scaffolds with high *in vivo* patency rates due to their low antigen content, retained native tissue basement membrane integrity and preserved native ECM structure, composition and functional properties.

*Corresponding author. griffiths.leigh@mayo.edu (L.G. Griffiths).

Declaration of Competing Interest

The authors declare that they have no known competing financial interests or personal relationships that could have appeared to influence the work reported in this paper.

Supplementary materials

Supplementary material associated with this article can be found, in the online version, at doi:10.1016/j.actbio.2021.06.034.

Keywords

Tissue engineering; Small diameter vessel; Extracellular matrix

1. Introduction

Cardiovascular disease (CVD) is the leading cause of death globally and is expected to affect over 40% of the population in the United States (US) by 2030 [1]. Diseases of small diameter blood vessels (i.e., < 6 mm, such as coronary artery diseases and peripheral vascular diseases) encompass the largest portion of CVDs, affecting over 25 million people in the US [2,3]. Despite a wide array of treatments, the use of autologous tissue remains the current standard of care for small diameter vessel disease with over 4.2 million people undergoing autologous vascular grafting every year [4–6]. However, autologous arterial and/or venous conduit harvest have been associated with donor site complications including limb or breast ischemia, impaired respiratory function, cellulitis, neuropathy, wound infection and non-healing wounds, increasing patient morbidity and reducing overall outcome[7–10]. Additionally, approximately one-third of patients are non-eligible for autologous vessel grafting due to lack of suitable donor vasculature caused by pre-existing vascular disease, amputation, previous vessel harvest or limited vessel length to meet the need of multiple grafts [11–19]. For instance, challenging cases of chronic venous insufficiency are optimally treated by venous valve replacement, where the best patient outcomes are seen with multiple valve transplants [20–23]. However, limited availability of upper extremity venous valves frequently prevents multiple valve transplant procedures, hindering the potential benefit of the surgery. Therefore, the development of an off-the-shelf vascular graft capable of eliminating the need for autologous vessel harvest, has potential to benefit over 1.4 million patients per yea.

Off-the-shelf small diameter vascular grafts have the potential to overcome the challenges associated with use of autologous vessels, as they offer sufficient length and unlimited availability. Acellular extracellular matrix (ECM) scaffolds derived from xenogeneic vascular tissue is an ideal source for off-the-shelf vascular grafts [24–26]. The ECM is a non-cellular, multi-scalar structure produced by the colocalization of functional and structural proteins secreted by host cells. These proteins are dynamically secreted in a tissue specific manner to fulfill tissue specific needs, resulting in a composite material with perfectly suited mechanical properties and signaling molecules to support normal vascular function and cell homeostasis [27]. Indeed, signaling molecules (e.g., growth factors, matrikines, matricryptic signals, microvesicles) within the native ECM environment are known to modulate cell adhesion, migration, proliferation and differentiation [28–33]. Consequently, the use of xenogeneic small diameter vascular ECM scaffolds has potential to provide a graft which recapitulates native vascular mechanical properties, while also informing pro-regenerative cellular responses, modulating graft turn-over and remodeling [28–34].

Significant interest in the production of xenogeneic ECM vascular grafts has resulted in intense research efforts towards the development of suitable grafts for small diameter

vascular replacement. Most research efforts have focused on development and/or improvement of decellularization techniques in attempts to produce immunologically acceptable ECM grafts that retained native ECM protein structure, composition and associated functional properties [35]. As a result, an extensive array of decellularization techniques of varying harshness have been developed. Such decellularization techniques result in considerably different degrees of antigen depletion and associated ECM deterioration [36–39]. The innumerable attempts at producing ECM vascular grafts via decellularization techniques have provided the field with valuable information regarding the *in vitro* and *in vivo* behavior of ECM vascular grafts, but unfortunately have not been capable of producing a patient-ready ECM graft for small diameter vessel disease. This is due to a wide array of failure mechanisms that affect xenogeneic ECM vascular grafts once implanted *in vivo*, including scaffold calcification, aneurysm, intimal hyperplasia, thrombosis and immune-mediated rejection [40–44].

The triggers for these failure mechanisms have been associated with the inefficiency of decellularization processing methods to effectively eliminate antigens from the biomaterials; their inability to avoid off-target disruption of the remaining structural and functional integral ECM proteins, as well as their high toxicity to repopulating cells even after extensive washout procedures [45–49]. Immune-mediated rejection has been shown to be dependent on the content of known (e.g., galactose 1–6 alpha galactose (α-gal), major histocompatibility complex (MHC)) and unknown (i.e., minor histocompatibility) antigens in the biomaterial after tissue processing [50]. However, the decellularization paradigm focuses on reducing the antigenic content of ECM grafts by removing only cellular components from candidate tissues [51–54]. Consequently, the decellularization approach fails to recognize the potential for remnant non-cellular antigens to trigger adaptive immune recognition and resultant graft failure [44,50,55,56].

All other vascular ECM scaffold failure mechanisms are caused by alterations to the graft structural and functional proteins. Altered mechanical properties, caused by damaged structural proteins, lead to compliance mismatch between the graft and native tissue, resulting in failure by calcification, aneurysm formation and/or development of intimal hyperplasia [42,44,57,58]. Alterations to the ECM functional proteins, such as basement membrane (BM) proteins, diminish the recellularization capacity of the ECM graft, reducing the potential for graft endothelialization, increasing thrombosis risk, which reduces patency rates and ultimately leads to graft failure [36,49,59]. Therefore, the success of small diameter vessel ECM grafts is completely dependent on the capability of the tissue processing method to significantly decrease the graft immunogenic content, while maintaining the native ECM proteins structure, composition and function [60].

Antigen removal (AR) is an alternative tissue processing method shown to significantly reduce antigenic content of xenogeneic tissues, while retaining native ECM structure, composition and function [50,61]. Previous comprehensive *in vitro* studies have demonstrated that the AR tissue processing is capable of retaining native vascular ECM protein structure and function when applied to small diameter (< 3.5 mm) bovine saphenous vein (SV), thereby maintaining native vascular mechanical properties [62]. Furthermore, an improved AR process employing aminosulfabetaine 16 (ASB-16) has recently been reported

to enhance elimination of lipophilic antigens from bovine pericardium, conferring *in vivo* adaptive immune tolerance toward the resultant scaffolds [50]. In the current manuscript, we hypothesize the improved ASB-16 based AR process will eliminate antigenic molecules from bovine saphenous vein grafts, conferring *in vivo* adaptive immune avoidance. We further hypothesize that retention of native ECM protein structure/function relationships in AR small diameter vascular scaffolds will foster *in vivo* cellular repopulation preserving graft patency and function. To test these hypotheses we developed two *in vivo* rabbit models, one to assess the pure immunogenic response to the material (subpannicular implant) and a second to assess the effect of preservation of basement membrane integrity on the function of the ECM scaffold as a small diameter vascular graft (jugular interposition).

2. Materials and methods

All animal procedures were performed in accordance with the Mayo Clinic IACUC and the NIH Guide for Care and Use of Laboratory Animals. All experiments were performed with $n = 6$ replicates per group, unless otherwise stated. Anatomically adjacent pieces from different animals ($n = 3$ per experiment) were evenly distributed across groups, unless otherwise stated. Expanded methods are available in the Supplemental material.

2.1. Tissue harvest

Fresh bovine saphenous veins (SV) were harvested from young adult cattle (15–24 months) and shipped on ice. Rabbit jugular veins (allografts) were harvested from recently deceased New Zealand white rabbits. Tissue was dissected to remove perivascular connective tissue and adventitia. Resultant SV and jugular veins were stored uncut in Dulbecco's Modified Eagle Medium (DMEM) with 15% (v/v) dimethyl sulfoxide (DMSO) at −80 °C.

2.2. Antigen removal

Small diameter (> 3.5 mm) tubular SV scaffolds, each approximately 10 cm in length, were processed in 30 mL of solution atRT by perfusion using peristaltic pumps at a flow rate of 10 ml/min and all solutions changed twice daily, unless otherwise stated. Biopsy punched scaffolds, 6 mm in diameter and 14 mm in diameter, were processed in 2 mL and 4 mL of solution, respectively,at RT in an orbital shaker at 150 rpm and all solutions changed twice daily, otherwise stated. All scaffolds were processed under sterile conditions inside a biosafety cabinet.

All AR solutions were added to a base buffer solution (0.5 mM Pefabloc, 1% v/v antibiotic antimycotic solution (AAS) in 10 mM Tris–HCl (pH 8.0). Antigen removal (AR) samples (scaffolds) underwent sarcomeric relaxation (3% amidosulfobetaine-16 (ASB-16), 120 mM potassium chloride (KCl), 4 mM $MgCl_2$, 4 mM EDTA, 5.88 mM Na-ATP, 10 mM 2,3 Butanedione monoxime (BDM), 0.5 mM Pefabloc and 1% AAS in 10 mM Tris–HCl, pH 7.6) two times for 30 min each. Relaxed veins were incubated in lipophilic protein solubilization solution (3% ASB-16 in 100 mM dithiothreitol (DTT), 2 mM $MgCl_2$ and 600 mM KCl, in base buffer) for 48h. AR-scaffolds underwent sarcomeric disassembly by washing in base buffer twice for 15 min, followed by incubation in 50 nM Latranculin B (Cayman Chemical) in base buffer for 2 h. Samples were washed again with base buffer

twice for 15 min and incubated for 2 h in 0.6 M KCl in base buffer. Washed a final time with base buffer twice for 15 min and incubated 2 h in 1 M potassium iodine (KI) in base buffer, followed by overnight incubation in base buffer alone. The KCl and KI steps were repeated the next day, followed by overnight incubation in base buffer. Scaffolds were then placed in lipophilic protein solubilization solution for 48 h, followed by 24 h incubation in hydrophilic protein solubilization solution (100 mM dithiothreitol (DTT), 2 mM $MgCl_2$ and 600 mM KCl, in base buffer). Subsequently, scaffolds underwent 24 h of nuclease digestion (10 Kunitz units/mL DNase I, 15 Kunitz units/mL RNase A, 0.5 mM Pefabloc, 1% AAS, 0.15 M NaCl, 5 mM $MgCl_2$–$6H_2O$ in10 mM Tris–HCl, pH 7.6)) and 96 h of washout in base buffer at 4°C. SDS-decellularization samples (SDS-scaffolds) were incubated in 1% w/v sodium dodecyl sulfate (Bio-Rad) in base buffer for 24 h, washed for 30 min in 1% v/v Triton-X 100 (Bio-Rad) in base buffer, followed by nuclease digestion for 24 h and washout for 92 h. Untreated-SV anatomical tissue controls and allograft controls were kept frozen at −80 °C. All samples were incubated overnight in 1% AAS in DMEM before implantation.

2.3. Anti-Untreated bovine saphenous vein serum production

New Zealand white rabbits ($n = 2$) received adjuvanted subcutaneous injections of homogenized SV and sera collected as previously reported for other tissues [64].

2.4. Residual protein extraction

Hydrophile and lipophile protein extracts were acquired by incubating manually minced AR-scaffolds, SDS-scaffolds and untreated SV anatomical controls (6 mm biopsy punches) in 0.1% and 1% sodium dodecyl sulfate, respectively. All extracts were stored at −80 °C [64]

2.5. One-Dimensional electrophoresis and western Blot

Global antigen content was assessed by probing all blots with rabbit poly-polyclonal anti-untreated SV serum and assessed for IgG positivity using mouse anti-rabbit IgG secondary antibody. Densitometry was determined using AlphaView image acquisition and analysis software, with all lanes corrected for background. Densitometry was used to sum the density of all bands in a particular sample lane and quantified in relative fluorescence units (RFU) [64,65].

2.6. Histology

Sample sections were stained with Hematoxylin and Eosin (H&E) and Picro-Sirius Red (PSR). Fibrotic capsule thickness and number of infiltrated non-immunogenic spindle cells were measured from H&E slides using a Nikon Eclipse E600 microscope. Fibrotic capsule was measure via the measurement tool in NIS-Elements Advanced Research software. Collagen birefringence was measured from PSR slides using polarized light and percent area of collagen alignment was calculated using MATLAB. For both fibrotic capsule and collagen birefringence, the median of the six measurements was plotted. For number of infiltrated non-immunogenic spindle cells, the median of four measurements was plotted.

For all fluorescent stains, paraffin embedded scaffold sections were deparaffinized, antigen retrieved, and non-specific binding was blocked. Rabbit anti-laminin antibody (1:20, Invitrogen, Carlsbad, CA) and rabbit anti-collagen IV antibody (1:200, Abcam) were used

to stain bovine laminin and collagen IV. Fluorescent anti-rabbit secondary antibody tagged with Alexa Fluor 647 (1:200, Abcam) and DAPI (ProLongTM Gold antifade reagent with DAPI, Invitrogen) were used for visualization. Rat anti–CD3 primary antibody (1:100, Abcam) was utilized for lymphocyte staining. Rat anti-MAC 387 antibody (1 μg/ml, Abcam) was used for macrophage staining. Mouse anti-PECAM-1 antibody (2 μg/ml, Abcam) was used for PECAM-1 staining. Fluorescent anti-rat secondary antibody tagged with Alexa Fluor 546 (1:200, Abcam), anti-mouse secondary antibody tagged with Alexa Fluor 647 (1:200, Abcam) and DAPI (ProLongTM Gold antifade reagent with DAPI, Invitrogen) were used for visualization. For all stains, slides were imaged using a Nikon Eclipse E600 microscope and digital images collected. Quantification of fluorescent images was performed on six randomly selected fields of view per sample and analyzed in MATLAB.

2.7. Quantitative biochemistry

DNA content was quantified from dry tissue using Quant-iT PicoGreen assay kit following the manufacturer's protocol and as previously reported.

2.8. Subpannicular scaffold implantation-Immunogenic model

New Zealand White rabbits (4 groups, $n = 6$ per group), underwent subpannicular implantation of rabbit jugular vein (allograft), untreated SV, AR-scaffolds and SDS-scaffolds. A single skin incision was made and subpannicular tissues undermined, creating four pockets, two on either side of the spine. Each rabbit had identical 1 × 1 cm samples from a single group placed in each of the four pockets, and the incision closed routinely. At day 56, all rabbits were euthanized and one sample excised en-bloc and fixed for histology. The other 3 implants were stored at −80 °C for later analysis.

2.9. Endothelial recellularization capacity

GFP-labelled human umbilical vein endothelial cells(GFP-HUVEC, Angio-Proteomie, Boston, MA) were expanded to P4 in a *T*-25 flask coated with Quick coating solution (Angio-Proteomie) at 37 °C, 5% CO_2. Cells were cultured in 6 mL of endothelial cell growth medium (Lonza, Allendale, NJ) being changed 24 h after thawing and once every other day thereafter. Cells were lifted using Accutase® solution. Scaffolds (14 mm in diameter) were sutured on to high temperature foam to avoid scaffold recoil and incubated in 1% AAS in endothelial cell media overnight before seeding. A 3.5 mm in diameter glass cylinder was used to seed GFP-HUVECs, at a density of 600 cells/mm^2, in a circular shape on ECM scaffolds. Cells were allowed to adhere for 6 h in 50 μL of cell media. After the adhesion period, cells were unconfined and cultured in 1 mL of endothelial cell media. Cells were imaged using inverted microscopy (Nikon Eclipse Ts2R) with large scan function stitching between 35 and 40 4x magnification images at days 3 and 8 post seeding. Recellularization capacity was assessed qualitatively for both groups at days 3 and 8 post-seeding.

2.10. Jugular interposition implantation-vascular conduit function model

New Zealand White rabbits (4 groups), underwent jugular interposition of rabbit jugular vein (autograft, ($n = 5$), untreated SV ($n = 6$), and AR-scaffolds ($n = 11$)). The rabbits

receiving the AR-scaffolds were divided into two groups, a basement membrane (BM) group with the lumen of the vessel facing the blood flow ($n = 6$) and a non-basement membrane (NBM) with the ablumen of the vessel facing the blood flow ($n = 5$, i.e., the tubular scaffold was turned inside-out). Since re-sizing of the scaffold was required to match the diameter of the graft to the rabbit jugular diameter, such inverting of the vessel was accomplished without any damage to the scaffold. The adventitia from the NBM scaffolds was carefully and completely removed until the tunica media was exposed and no “loose” fibers were observed under a surgical microscope at 12.5X magnification.

Blood was drawn pre– and post- implantation, serum isolated as previously reported and stored at −80 °C [64]. A skin incision in the ventral midline of the cervical region was made and the left and right jugular veins were isolated, and the perivascular tissue was removed. For the autograft group, a section of jugular vein was harvested from the native jugular tissue prior to performing the interposition procedure. For the other groups, a long tubular bovine SV conduit was interposed between the cut ends of the jugular vein. For all groups the veins were implanted using end-to-end anastomosis, at both the proximal and distal ends of the transected vessel. Skin and underlying tissues were closed routinely. At day 35, all rabbits were euthanized and both samples were excised en-bloc and stored at −80 °C for later analysis. At the time of en-bloc resection, the proximal side of the native vessel was canulated above the anastomosis site and the vessel was perfused with saline. The patency rate of the vascular scaffolds was determined by the visualization of the outflow of saline at the distal end of the implant.

2.11. Gene expression analyses

For gene expression analysis, a 2 mm long circumferential slice from the middle of the implanted scaffolds was cut, frozen in liquid nitrogen and manually pulverized with pestle and mortar. RNA extraction from pulverized scaffolds was performed using TRIzol, following the manufacturer’s protocol with two modifications (See Appendix). qPCR was run in triplicates with TaqMan™ Gene Expression Master Mix. The samples were amplified for 45 cycles in an ABI Quant qPCR machine and the amount of cDNA on each sample was normalized to Beta-Actin housekeeping gene.

2.12. Recipient graft-specific antibody titer

As previously reported, homogenized untreated SV was bound to a 96-well plate and probed with sera from jugular interposition rabbits collected on days 0, 14, 21, 28 and 35 post implantation (Autograft $n = 5$, untreated SV $n = 6$, BM $n = 6$ and NBM $n = 5$). For visualization, the plates were incubated with Horseradish peroxidase (HRP) conjugated mouse anti-rabbit secondary antibody and 3,3',5,5'-Tetramethylbenzidine (TMB) substrate and absorbance was read at 450 nm. Linear regression of the reference curve (day 0 pooled rabbit serum) was used to determine the graft-specific production of antibodies. Titers from days 7, 14, 21, 28, and 35 were normalized to day 0 pooled rabbit sera to give fold-change relative to baseline for each rabbit/time point [66].

2.13. Blinded veterinary pathology review

A blinded review of H&E slides by a board-certified veterinary pathologist categorized the morphological change in bovine SV subcutaneous and interposition implants in leporine subjects using a semi-quantitative scale.

2.14. Statistical analysis

All data were analyzed for outliers using ROUT method with $Q = 1\%$, followed by analysis Wilcoxon/Kruskal-Wallis Test with Dunn *post-hoc* analysis on non-parametric medians [4]. ELISA analysis was conducted using repeated measures two-way ANOVA and Tukey-Kramer HSD post-hoc analyses on standard least squares means. All data are expressed as median ± interquartile range (IQR). Statistical significance is defined at $p < 0.05$.

3. Results

3.1. AR significantly reduces resultant ECM scaffold cellularity and antigen content

Qualitative analysis of histological images revealed both AR and SDS-decellularization generated acellular SV scaffolds as determined by the complete absence of visible nuclei on H&E stained sections (Fig. 1A). Cellular content was further quantified by assessment of residual DNA content. Both AR (0.012 μg/mg, $p < 0.01$) and SDS (0.017 μg/mg [0.001–0.02], $p < 0.05$) scaffolds contained significantly lower levels of DNA than untreated SV (7.6 μg/mg [2.92–10.3], Fig. 1B). Total unknown minor histocompatibility content of AR, SDS and untreated SV were assessed via western blotting (Fig. 1C). AR (3.22 RFU [1.88–3.75], $p < 0.001$) significantly reduced unknown hydrophilic antigen content when compared to untreated SV (138.6 RFU [90.7–176.8]). Although SDS reduced hydrophilic antigens to very low levels (8.68 RFU [5.45–11.77], $p = 0.155$, Fig. 1D), this finding failed to reach statistical significance compared to untreated SV. Conversely, both AR (14.54 RFU [11.58–22.09], $p < 0.01$) and SDS (25.88 RFU [5.1–81.72], $p < 0.05$) reached statistical significant reduction of unknown lipophilic antigen content when compared to untreated SV (444.4 RFU [336.9–534.2], Fig. 1E).

3.2. AR preserves the macromolecular structure of ECM structural and basement membrane components

Preservation of native SV macromolecular structural protein organization and basement membrane integrity in ECM scaffolds was assessed using histology, immunofluorescent stains and polarized light microscopy. H&E-stained sections demonstrated ECM morphology was well preserved in AR scaffolds, while SDS-decellularization resulted in abluminal collagen fragmentation and the merging of collagen bundles throughout the scaffold (Fig. 2A). AR scaffolds retainednativeSV basementmembranecontentand organization as assessed by collagen IV and laminin immunofluorescence (Fig. 2B, C). Conversely, basement membrane protein content was visibly reduced in SDS-decellularized scaffolds when compared to untreated SV (Fig. 2B, C). Similarly, AR retained native collagen macromolecular structure as assessed by collagen birefringence (19.1% area [17.64–20.58], $p > 0.999$) when compared to untreated SV (17.86% area [15.36–21.47], Fig.

2D, E). By comparison, SDS-decellularization significantly reduced collagen birefringence (14.16% area [13.35–14.98], $p < 0.05$) when compared to untreated SV (Fig. 2E).

3.3. *AR scaffolds foster adaptive immune response avoidance, innate immune self-recognition and pro-regenerative cell infiltration in subpannicular* in vivo *model*

Adaptive immune response towards the scaffolds implanted subpannicularly was assessed via histomorphometry and quantification of $CD3^+$ cell presence. AR-scaffolds (3 Lymphocytes/scaffold cut edge [2–11], $p < 0.05$) resulted in the lowest lymphocyte infiltration, when compared to the other groups having significantly less lymphocyte infiltration than untreated SV (Fig. 3A, G, $p < 0.01$). Allograft (10 Lymphocytes/scaffold cut edge [10–18]) and SDS-decellularized scaffolds (13 Lymphocytes/scaffold cut edge [5–32], Fig. 3G) resulted in mild to moderate levels of lymphocyte infiltration. Alternatively, untreated SV (20 Lymphocytes/scaffold cut edge [12–44]) experienced the highest number of lymphocyte infiltration, when compared to the other groups. Compared to levels of fibrotic encapsulation in the allograft group (19.96 μm [15.7–36.2]), no evidence of foreign body type innate immune response towards AR-scaffolds (27.4 μm [12.8–46], Fig. 3H) was seen, with minimal fibrotic encapsulation found around these implants. Although not statistically different from Allograft, increased fibrotic encapsulation was found around untreated SV (54.03 μm [40.3–69.2]), while SDS-decellularized scaffolds (94.8 μm [37.4–110.1]) experienced a statistically increased level of fibrotic encapsulation compared to Allografts ($p < 0.05$).

Differently, H&E stained images demonstrated an increased pro-regenerative response towards AR-scaffolds as evidenced by the high number of non-immune spindle shaped cells infiltrating the scaffolds (20 infiltrating cells [2–24]), similar to those found in allograft scaffolds (37 infiltrating cells [20–64]). Alternatively, when compared to allografts both untreated SV (2 infiltrating cells [1–2]) and SDS (1 infiltrating cells [0–2]) scaffolds had significantly lower infiltrating spindle shaped cells (Fig. 3B–E, I). Furthermore, polarized PSR images demonstrated that infiltration of these cells into AR scaffolds was associated with ECM reabsorption and turnover as evidenced by removal of mature polarizing collagen at the periphery of the scaffold, and replacement with newly formed nonpolarizing collagen (Fig. 3F). All other groups failed to show any evidence of either non-immune cell infiltration or matrix turnover, with scaffold polarization remaining unchanged compared to pre-implantation levels.

3.4. AR scaffolds attains increased endothelial recellularization capacity as well as increased cell modulatory capacity via the retained basement membrane proteins

Scaffold recellularization capacity and effect of basement membrane presence vs. absence on cell migration was qualitatively assessed for AR and SDS scaffolds. No qualitative difference in cell behavior and morphology was detected in any of the groups 3 days after seeding (Fig. 4A, C, E, G). Differences in cells quantity, morphology and behavior were observed at day 8 post-seeding (Fig. 4B–D, F, H). Number of cells present on both BM (Fig. 4F) and NBM (Fig. 4H) SDS scaffolds at day 8 decreased when compared to the earlier time point (day 3, Fig. 4E, H), Conversely, number of cells on BM (Fig. 4B) and NBM (Fig. 4D) surface of AR scaffolds was not diminished at the day 8 time point (Fig. 4B, D).

Additionally, the effects of basement membrane proteins on HUVECs spread (migration + proliferation) were assessed by seeding cells in the presence (BM) or absence (NBM) of basement membrane proteins. No differences in cell spread were seen between the groups at day 3. HUVECs seeded on the AR BM scaffolds were able to spread more and covered a larger surface area than the cells on scaffolds from the other groups at day 8 post-seeding (Fig. 4B), even when compared to the cells in the AR NBM scaffolds (Fig. 4D).

3.5. *AR scaffolds reduce humoral immune response and maintain lumens patency in jugular interposition* in vivo *model*

To determine the effect of basement membrane proteins on *in vivo* recellularization capacity (e.g., endothelialization) and functionality (e.g., patency) of small diameter vascular grafts, we employed a rabbit jugular interposition model. Due to the inability of SDS tissue processing to retain important ECM proteins (e.g., basement membrane proteins (Fig. 2)) andsupportendothelialcell growth (Fig. 3), the SDS group was eliminated from these experiments. Instead, one AR scaffold group was implanted with the basement membrane proteins facing the blood flow (BM group), while the other was implanted with the non-basement membrane side facing the blood flow (NBM group). All interposition grafts were technically successful as demonstrated by evidence of intragraft flow immediately after the interposition procedure (Fig. 5A). All animals survived to the end of the study.

Gross pathological images of the neck of the rabbits at the time of explantation demonstrate the location of the implanted grafts (arrows) and the number, size and distribution of dilated collateral vessels (arrowheads, Fig. 5B). In the Autograft group the vascular lumen remained fully patent and no evidence of collateral vessel dilation was observed (Fig. 5B and C). A small number of mildly dilated collateral vessels were present in the Basement Membrane protein (BM) group, despite the graft lumen being patent in all cases. Conversely, in the untreated SV and Non-Basement Membrane brane protein (NBM) groups extensive occlusion of the vascular luminal by fibro-thrombotic plaque and a large number of prominently dilated collateral vessels was observed in all cases. Patency rate of the scaffolds was determined by cannulation and perfusion of the graft. 5/5 Autograft scaffolds were determined to be patent, 3/6 untreated SV scaffolds being patent, 6/6 BM scaffolds being patent and 1/5 NBM scaffolds being patent (Fig. 5D).

Graft-specific adaptive immune response was quantified using longitudinal assessment of graft-specific IgG production (Fig. 5E). A significant increase in graft-specific antibody production towards all bovine scaffolds (**Untreated SV:** 53.7 fold change [28.5–68.5], $p < 0.01$, **BM:** 13.7 fold change [8.71–14.2], $p < 0.001$ and **NBM:** 13.4 fold change [9.59–14.1], $p < 0.01$), compared to Autografts (1.62 fold change [1.43–2.04]) was first detected on day 21. Graft-specific antibody production towards AR-scaffolds plateaued by day 28, with no statistical difference when compared to itself between day 28 (**BM:** 78.4 fold change [57.7–89.6], $p > 0.05$ and **NBM:** 73.1 fold change [50.7–79.1], $p > 0.05$) and day 35 (**BM:** 83.2 fold change [78.6–103] and **NBM:** 78.9 fold change [73.3–114]). Conversely, antibody production toward untreated SV scaffolds continued to increase over time reaching a maximum of 230 fold change [104–326] by day 35. Maximal graft-specific antibody titer was significantly higher for untreated SV than that towards AR-scaffolds (**BM:** 83.2

antibody fold change [78.6–103], $p < 0.05$ and **NBM:** 78.9 antibody fold change [73.2 –114], $p < 0.05$) and Autografts (0.798 antibody fold change [0.387–1.8], $p < 0.01$).

3.6. *AR scaffolds achieve high patency rates in jugular interposition* in vivo *model*

Explanted jugular interposition grafts were sectioned and mid-graft circumferential H&E slides examined by a board certified veterinary pathologist. Luminal area was measured showing that Autograft (1.96 mm^2 [1.18–4.51], $p < 0.05$) and BM scaffolds (1.66 mm^2 [0.665–2.24], $p < 0.05$) having significantly larger open lumen area when compared to NBM scaffolds (0 mm^2 [0–0.215]). No significant difference in lumen area was seen between any of the other groups, including untreated SV scaffolds (0.5 mm^2 [0.05–1.32], Fig. 6B). Adaptive immune response towards the scaffolds implanted as jugular interposition was assessed via quantification of immunofluorescent stains of CD3 (Figs. 6C, Suppl. 1). Macrophage presence was quantified using MAC 387 immunofluorescence staining (Fig. 6D). Both AR-scaffolds (BM and NBM) stimulated a robust cell-mediated adaptive response resulting in increased lymphocyte (**BM:** 453 Lymphocytes/Scaffold area [322–550], $p < 0.05$ and **NBM:** 398 Lymphocytes/Scaffold area [263–514], $p < 0.05$) and macrophage (**BM:** 128 Macrophages/Scaffold area [82.3 –173], $p < 0.05$ and **NBM:** 205 Macrophages/Scaffold area [63–231], $p < 0.05$) infiltration when compared to Autografts (6 Lymphocytes/Scaffold area [1.5–51.5], 1 Macrophages/Scaffold area [1]). No significant difference in number of lymphocytes (316 Lymphocytes/Scaffold area [240–416], $p > 0.05$) and macrophages (75 Macrophages/Scaffold area [15–149], $p > 0.05$) in untreated SV scaffolds was found compared to either AR group.

To further quantify and identify the specific type of lymphocytes and macrophages infiltrating the scaffolds, the expression of a wide array of genes was examined via real-time qPCR. All bovine scaffolds experienced an increase in lymphocyte gene expression when compared to autografts (gene expression fold increase). Cells infiltrated into untreated SV scaffolds (2.7 Fold increase [0.44–9.31] expressed the highest amount of CD3 when compared with Autografts and both AR-scaffolds (**BM:** 1.6 Fold increase [0.273–5.89], **NBM:** 1.8 Fold increase [0.623–4.87]), however no statistical significance was found between the bovine groups (Fig. 6E). Similarly, the highest CD4 expression was also seen among the cells infiltrated into untreated SV (6.14 Fold increase vs. autografts [2.05–10.8]), exhibiting ~1.5 times more infiltrating cells than in the AR-scaffolds (**BM:** 3.34 Fold increase [2.57–9.57], **NBM:** 3.37 Fold increase [1.5–6.48]), however no statistical significance was found between the bovine groups (Fig. 6F). Differently, the highest CD8 expression was found in the cells infiltrating the BM scaffolds (2.25 Fold increase vs. autografts [1.52–6.81]) and ~1.4 times more than untreated SV scaffolds (1.74 Fold increase [1.24–3.9]) and NBM scaffolds (1.69 Fold increase [0.753–5.57]), however no statistical significance was found between the bovine groups (Fig. 6G). Similarly, gene expression for regulatory T cells (FOXP3) was highest in BM scaffolds (22.8 Fold increase [14.8–28.3]) when compared to Autograft and around 1.3 times more than that produced in the untreated SV scaffolds (13.3 Fold increase [4–85.7]) and NBM scaffolds (17.2 Fold increase [11.6–35.4]), however no statistical significance was found between the bovine groups (Fig. 6H).

Similar to lymphocyte gene expression, all bovine scaffolds experienced an increase in macrophage gene expression (CD163) when compared to Autografts (gene expression fold increase). Cells infiltrating the BM scaffolds (16.3 Fold increase vs. Autograft [5.87–18.2]) expressing the highest amount of CD163, ~1.5 times more than that of untreated SV scaffolds (9.67 Fold increase [8.36–12.9]) and NBM scaffolds (8.82 Fold increase [4.53–12]), however no statistical significance was found between the bovine groups (Fig. 6I). In an attempt to determine the polarization of the macrophages infiltrating the scaffolds, gene expression of characteristic M1 (TNFα) and M2 (MRC1) markers were analyzed. Once more, all bovine scaffolds presented an increase in both TNFα (**untreated SV:** 9.29 Fold increase [1.95–16.7], **BM:** 7.64 Fold increase [5.05–14.5], **NBM:** 6.23 Fold increase [5.23–18], Fig. 6J) and MRC1 (**untreated SV:** 2.28 Fold increase [1.09–2.58], **BM:** 2.77 Fold increase [0.936–3.67], **NBM:** 1.67 Fold increase [1.22–2.25], Fig. 5K) gene expression when compared to autografts, but no difference was seen among the bovine groups.

3.7. *Basement membrane components are critical to fostering* in vivo *endothelial cell repopulation of AR scaffolds in the jugular interposition model*

Scaffolds recellularization capacity was determined by the degree of cell infiltration seen in H&E images and PECAM-1 staining to identify endothelial cell repopulation. Scaffolds BM group resulted in higher cell infiltration in their luminal surface and within the tunica media of the vascular scaffold, when compared to untreated SV and NBM scaffolds (Fig. 7A). Due to the presence of cells prior to the surgical procedure recellularization cannot be assessed for scaffolds in the Autograft group. Furthermore, the cells present in the luminal surface of the Autograft and some of the cells present in the BM scaffolds colocalized with platelet endothelial cell adhesion molecule (PECAM-1) indicating these were endothelial cells (Fig. 7B). BM scaffolds experienced the most endothelial cell repopulating on luminal surface of the scaffold (41 PECAM-1^+ cells/mm [11–61]) when compared to the other bovine scaffolds groups (**untreated SV**: (1 PECAM-1^+ cells/mm [0–19], $p < 0.05$) and **NBM scaffolds**: 0 PECAM-1^+ cells [0–0], $p < 0.001$). Due to the non-parametric statistics the number of endothelial cells found in the lumen of the BM scaffolds was not statistically different than that of the Autograft group(114 PECAM-1^+ cells/mm [101–320]) despite the absolute number being noticeably lower (Fig. 7C).

4. Discussion

Acellular extracellular matrix scaffolds derived from xenogeneic vascular tissues are an attractive source of biomaterials for off-the-shelf small diameter vascular grafts. The overwhelming adaptive immune response toward xenoantigens drives the primary focus of the field, whose primary objective is to reduce the antigenic content of the tissue to a level where it does not activate an adaptive immune response (below-threshold antigenicity) and thus avoid adaptive immune-mediated graft destruction [50,55,66]. However, achieving below-threshold antigenicity has been elusive, resulting in premature graft failure and preventing study of other important factors which modulate in vivo graft success [56,67,68]. Consequently, progress in overcoming other known failure mechanisms has been limited by antigenicity related responses. The results of this study demonstrate the possibility of achieving below-threshold antigenicity of xenogeneic scaffolds and highlight the critical

importance of doing so while maintaining the composition, structure and function of integral ECM components to foster recipient pro-regenerative responses.

As mentioned previously, Antigen Removal (AR) is a tissue processing method employing protein chemistry principles of differential stepwise solubilization to reduce antigenic content of xenogeneic scaffolds [66]. When applied here to bovine SV, AR employing ASB-16 reduced the global antigenic content by >96%, surpassing the previously reported threshold required for achieving *in vivo* adaptive immune avoidance (i.e., >92%) for other tissues (e.g., bovine pericardium) [50]. Indeed, *in vivo* testing of AR bovine SV scaffolds in long term (56 days) immunogenic animal model (subpannicular implantation) demonstrated significantly reduced lymphocyte infiltration compared to untreated SV tissue. These results highly contrast previously reported decellularization findings in which ECM grafts or some of its derivatives are seen to elicit strong immunogenic responses caused by remnant antigens that lead to material failure [69–74]. Adaptive immune avoidance of AR-scaffolds was further seen in the jugular interposition model, where antibody production towards AR-scaffolds was reduced by >60% when compared to untreated SV. Circulating antibodies play a key role in scaffold degradation as they are capable of binding to biomaterials, activating complement and recruiting immune system cells to aid in scaffold degradation [75]. Therefore, significant reduction of antibody production towards AR-scaffolds is an extremely important achievement of AR tissue processing. However, it is important to point out that although antibody production towards AR-scaffolds was low, it still failed to achieve levels observed for Autografts.

Additionally, in the vascular interposition model the number of lymphocytes and macrophages infiltrating AR-scaffolds were significantly higher than those seen in Autografts. The discrepancy in number of infiltrating lymphocytes in AR-scaffolds in the subpannicular vs. the jugular scaffolds can be explained by one of two possible mechanisms. Post-surgical inflammatory response due to the short timeframe for jugular interposition (35 days) versus the longer subpannicular model (56 days) may be responsible of the increased number of lymphocytes seen in the jugular vs. subpannicular AR-scaffolds. Post-surgical inflammation is characterized by the successive pathological expression of nervous, immune and endocrine system responses, collectively known as the phases of the inflammatory response [76]. During the first or nervous phase, active vasoconstriction and vasodilation achieve reperfusion to the damaged area, as well as increased endothelial permeability [77–79]. The intermediate phase or immune phase is characterized by cell migration and tissue infiltration by inflammatory cells [76,80]. The last or endocrine phase results in tissue remodeling and wound healing, with lymphocytes and macrophages being the predominant cell types found within the injured tissue [76,80]. Being on the last phase of the post-surgical inflammatory responseis one possible explanation for the increased macrophage and lymphocyte infiltration into jugular AR-scaffolds.

The second mechanism that could explain the differential cell infiltration between subpannicular and jugular scaffolds, is the difference in implantation sites and their different microenvironmental conditions. Subpannicular implantation is an attractive immunogenic animal model due to easy implantation and harvest of biomaterials. Being a minimally invasive surgery, it minimizes tissue damage and post-surgical inflammation that might

obscure the true antigenic response towards the biomaterial [81]. However, it has been demonstrated that implants in the subpannicular space are poorly vascularized and therefore are minimally exposed to either endothelial cells or the process of angiogenesis, which are both highly capable of inflammatory response modulation and perpetuation [81,82]. On the other hand, the scaffolds implanted as jugular substitutes were in constant and direct contact with endothelial cells and experienced significant angiogenesis (Suppl. Fig. 2). Exposure to both, endothelial cells and the process of angiogenesis is therefore a potential explanation for the increased local immune response towards the jugular scaffolds. However, the fact that antibody production towards AR-scaffolds had started to plateau between days 27 and 35 post-implantation while antibody production towards untreated SV scaffolds kept increasing suggests the systemic immune response towards the AR-scaffolds had reached its peak (<40% of that seen toward untreated SV tissue). Plateauing humoral immune response by day 28 supports the explanation that increased cell infiltration (lymphocytes and macrophages) in jugular scaffolds is likely due to a localized response due to post-surgical inflammation rather than persistent adaptive immune activation. However, future studies with longer jugular implantation times are needed to confirm this hypothesis.

Avoidance of innate immune pro-inflammatory responses is critical to successful in vivo application of vascular xenogeneic ECM scaffolds, since inflammatory responses ultimately result in degradation of ECM proteins leading to graft failure by aneurysm, intimal hyperplasia and calcification. The innate immune system recognizes non-self molecules and triggers a rapid secretion of chemokines and cytokines that drives a pro-inflammatory immune response [83]. Alterations or modifications to ECM proteins by harsh tissue processing methods result in the exposure of non-self ECM modifications (e.g., denaturation), serving as triggers for innate immune system activation and targets for immune destruction [84–87].

Achieving sufficient antigen elimination to overcome adaptive immune recognition, while simultaneously retaining native ECM protein macromolecular structure to avoid innate pro-inflammatory recognition has been the biggest challenge for current tissue processing methods [88]. For example, sodium dodecyl sulfate (SDS) is an ionic detergent widely used for xenogeneic tissue processing and ECM scaffold production [89–91]. Its broad use has provided a plethora of information regarding the decellularization performance of this detergent, as well as mounting evidence demonstrating its capability of denaturing ECM proteins throughout the ECM scaffold generation process [35–37,89–91]. Collagen, in particular, is highly susceptible to alterations by SDS due to its capacity to intercalate and unfold the collagen triple helical structure, denaturing the protein [92,93]. Accordingly, the scaffolds obtained via SDS treatment for this manuscript resulted in significant collagen denaturation, with collagen birefringence being reduced by > 20% when compared to untreated SV scaffolds. Scavenger receptors (e.g., SR-A) exhibit affinity for denatured collagen and are capable of orchestrating the selective adhesion of macrophages to denatured proteins [63,94,95]. Once adhered, activated vated macrophages secrete pro-fibrotic factors, modulating fibroblast behavior and resultant formation of a fibrotic capsule around the SDS-scaffolds [96]. The fibrous encapsulation of SDS-treated scaffolds observed in the current work is not unique. Indeed, this finding has been a recurrent problem broadly reported in the literature, that has hindered the advancement of ECM xenogeneic scaffolds

for vascular and other applications [57,66,96–103]. Conversely, the AR-scaffolds resulted in little to no fibrosis capsule formation around the implants, comparable to that of Allografts. This finding indicates the macromolecular structure of ECM proteins in AR-scaffolds are recognizable as “self” by the innate immune system and therefore result in a response which is comparable to that found in allograft tissue. Fibrosis avoidance is an important achievement of AR tissue processing method, as it overcomes a recurrent and previously unsolved problem in the field of vascular ECM scaffold generation and tissue engineering.

In addition to avoiding activation of pro-inflammatory innate immune responses, retention of native ECM composition, structure and function also poses significant advantages towards eliciting pro-regenerative responses. ECM proteins are involved in a wide array of biological processes including cell behavior, proliferation, migration, differentiation and wound healing [104]. Indeed, retention of native tissue ECM macromolecular structures by the AR tissue processing method elicited *in vivo* pro-regenerative responses in the current study [62]. Presence of unaltered ECM proteins in the AR-scaffolds implanted subpannicularly modulated increased infiltration of non-immune spindle shaped cells, which were not present in any of the other groups. Furthermore, it is likely that these spindle shaped cells reacted to the native ECM configuration of AR-scaffolds and are responsible for the observed pro-regenerative ECM reabsorption and scaffold turnover (Fig. 3D).

In more complex *in vivo* physiological environments, however, the performance of ECM scaffolds not only depends on the retention of structural ECM proteins, but also on the retention of their specialized functional ECM proteins. In vascular grafting, the presence of basement membrane proteins within the vascular structure is thought to be an absolute necessity for graft success [105]. Laminin and collagen IV (Col IV) are two particularly important basement membrane proteins due to their chemotactic properties, which modulate endothelial cell adhesion, migration and repopulation into the ECM [106–108]. The retention of basement membrane proteins in AR-scaffolds, including laminin and Col IV, conferred important effects on resultant endothelial cell repopulation and thrombosis avoidance of AR vascular implants.

AR vascular grafts implanted with their basement membrane proteins facing the lumen and blood flow (BM-scaffolds) resulted in high cellular infiltration, endothelial cells lining the lumen of the scaffolds and high patency rates (100% patency). Alternatively, AR vascular grafts implanted with their non-basement membrane protein containing surface facing the lumen and blood flow (NBM-scaffolds) resulted in negligible cell infiltration, complete absence of endothelialization and low patency rates due to scaffold thrombosis (20% patency). Achieving 100% patency rate of 2 mm in diameter, denuded ECM scaffolds under the extremely stringent venous flow environment to our knowledge has not been previously reported. In comparison, the patency rates reported in the literature for denuded ECM vascular scaffolds implanted in the arterial system are only 0–60%, even when exposed to the higher arterial blood flow velocity which is known to ameliorate failure by thrombosis [42,57,73,109]. Patency rates >60% have only been reported for ECM scaffolds implanted as arteriovenous fistulas (where flow rates are even higher than in the arterial system) or for scaffolds that have been seeded with endothelial cells or chemically coated prior to implantation [110–112]. For instance, heparin crosslinking is a commonly used coating

known to significantly reduce surface thrombogenicity of ECM vascular scaffolds, and has been reported to achieve patency rates of around 80% [113]. However, both cell seeding and chemical coating impede the much-desired off-theshelf characteristic of the vascular grafts. Retained basement membrane proteins, therefore, played an important role in achieving high AR-scaffold patency rates by avoiding thrombosis, and modulating endothelial and non-endothelial cell repopulation.

Endothelial cell repopulation of ECM vascular scaffolds is an absolute condition for long-term graft patency and proper vessel function. Endothelial cells are responsible of maintaining the dynamic equilibrium between prothrombotic and anti-thrombotic surfaces via protein secretion, thereby maintaining vessel homeostasis [114]. Endothelial cells further control thrombosis by acting as a physical barrier between subendothelial proteins (e.g., collagen and elastin), platelets and coagulation factors. Therefore, the lack of endothelialization present in NBM-scaffolds likely caused the formation of fibro-thrombotic plaques tightly adhered to the wall of the scaffolds, which partially or completely occluded the lumen of the vessel. Alternatively, the high patency rate in the BM-scaffolds can be attributed to the cell layer lining the lumen of the scaffolds. Although the morphology of these cells is not characteristic of mature endothelial cells, which can be attributed to the early stages of the repopulation process, PECAM-1 secretion (Fig. 7A) indicates these cells are indeed endothelial in origin. Longer time points would be needed to define both endothelial cell maturation in the lumen and cell penetration to deeper layers of the graft. Small thrombi were found in the BM-scaffolds, they were not adhered to the wall of the scaffolds but to the anastomosis site (Suppl. Video 1). This finding was considered to be due to the mild stenosis caused at the anastomosis site due to technical failure to consider the differences in vascular wall thickness between the graft and native vessel. Consequently, we conclude that the intact BM of AR-scaffolds confers a strongly positive effect on endothelial cell repopulation and thrombosis avoidance.

5. Conclusion

The results in this manuscript demonstrate the capability of AR tissue processing method to significantly reduce tissue antigenic content, while retaining the structure, function and composition of the ECM proteins in vascular scaffolds. Both of these characteristics translate into the capability of ECM vascular scaffolds of avoiding a pro-inflammatory immune response (adaptive and innate) and eliciting a pro-regenerative response, resulting in lack of failure and high patency rate of ECM small diameter (<3 mm) vascular grafts when implanted as jugular substitutes.

Supplementary Material

Refer to Web version on PubMed Central for supplementary material.

Acknowledgments

The authors would like to acknowledge the help of Jennifer Brazzell (IDEXX bioanalytics pathologist) the board certified veterinary pathologist who was responsible for grading the histology results in this manuscript.

Funding sources

This work was supported by the National Institutes of Health [Grant No. R01HL121086] and Minnesota Regenerative Medicine [Grant No. RMM 091718 DS 003].

References

[1]. Heidenreich PA, Trogdon JG, Khavjou OA, Butler J, Dracup K, Ezekowitz MD, Finkelstein EA, Hong Y, Johnston SC, Khera A, Lloyd-Jones DM, Nelson SA, Nichol G, Orenstein D, Wilson PW, Woo YJ, C. American Heart Association Advocacy Coordinating, C. Stroke, R. Council on Cardiovascular, Intervention, C. Council on Clinical, E. Council on, Prevention, A. Council on, Thrombosis, B. Vascular, C. Council on, C. Critical, Perioperative, Resuscitation, N. Council on Cardiovascular, D. Council on the Kidney in Cardiovascular, S. Council on Cardiovascular, Anesthesia, C. Interdisciplinary Council on Quality of, and R. Outcomes, Forecasting the future of cardiovascular disease in the United States: a policy statement from the American heart association, Circulation 123 (8) (2011) 933–944. [PubMed: 21262990]

[2]. Benjamin EJ, Muntner P, Alonso A, Bittencourt MS, Callaway CW, Carson AP, Chamberlain AM, Chang AR, Cheng S, Das SR, Delling FN, Djousse L, Elkind MSV, Ferguson JF, Fornage M, Jordan LC, Khan SS, Kissela BM, Knutson KL, Kwan TW, Lackland DT, Lewis TT, Lichtman JH, Longenecker CT, Loop MS, Lutsey PL, Martin SS, Matsushita K, Moran AE, Mussolino ME, O'Flaherty M, Pandey A, Perak AM, Rosamond WD, Roth GA, Sampson UKA, Satou GM, Schroeder EB, Shah SH, Spartano NL, Stokes A, Tirschwell DL, Tsao CW, Turakhia MP, VanWagner LB, Wilkins JT, Wong SS, Virani SS, E. American Heart Association Council on, C. Prevention Statistics, and S. Stroke Statistics, Heart disease and stroke statistics-2019 update: a report from the American heart association, Circulation 139 (10) (2019) e56–e528. [PubMed: 30700139]

[3]. Fryar CD, Chen TC, Li X, Prevalence of uncontrolled risk factors for cardiovascular disease: United States, 1999–2010, NCHS Data Brief. (103) (2012) 1–8.

[4]. Alexander JH, Smith PK, Coronary-artery bypass grafting, N. Engl. J. Med. 374 (20) (2016) 1954–1964. [PubMed: 27192673]

[5]. Slovut DP, Lipsitz EC, Surgical technique and peripheral artery disease, Circulation 126 (9) (2012) 1127–1138. [PubMed: 22927475]

[6]. Vacanti JP, Langer R, Tissue engineering: the design and fabrication of living replacement devices for surgical reconstruction and transplantation, Lancet 354 (Suppl. 1) (1999) S32–S34.

[7]. Lavee J, Schneiderman J, Yorav S, Shewach-Millet M, Adar R, Complications of saphenous vein harvesting following coronary artery bypass surgery, J. Cardiovasc. Surg. 30 (6) (1989) 989–991 (Torino).

[8]. Paletta CE, Huang DB, Fiore AC, Swartz MT, Rilloraza FL, Gardner JE, Major leg wound complications after saphenous vein harvest for coronary revascularization, Ann. Thorac. Surg. 70 (2) (2000) 492–497. [PubMed: 10969669]

[9]. Garland R, Frizelle FA, Dobbs BR, Singh H, A retrospective audit of long-term lower limb complications following leg vein harvesting for coronary artery bypass grafting, Eur. J. Cardiothorac. Surg. 23 (6) (2003) 950–955. [PubMed: 12829071]

[10]. Hillis LD, Smith PK, Anderson JL, Bittl JA, Bridges CR, Byrne JG, Cigarroa JE, DiSesa VJ, Hiratzka LF, Hutter AM, Jessen ME, Keeley EC, Lahey SJ, Lange RA, London MJ, Mack MJ, Patel MR, Puskas JD, Sabik JF, Selnes O, Shahian DM, Trost JC, Winniford MD, Jacobs AK, Anderson JL, Albert N, Creager MA, Ettinger SM, Guyton RA, Halperin JL, Hochman JS, Kushner FG, Ohman EM, Stevenson W, Yancy CW, and G. American College of Cardiology Foundation/American Heart Association Task Force on Practice, 2011 ACCF/AHA guideline for coronary artery bypass graft surgery: executive summary: a report of the American college of cardiology foundation/American heart Association task force on practice guidelines, J. Thorac. Cardiovasc. Surg. 143 (1) (2012) 4–34. [PubMed: 22172748]

[11]. Veith FJ, Moss CM, Sprayregen S, Montefusco C, Preoperative saphenous venography in arterial reconstructive surgery of the lower extremity, Surgery 85 (3) (1979) 253–256. [PubMed: 424995]

[12]. Edwards WS, Mohtashemi M, Holdefer WF Jr., The importance of proper caliber of lumen in femoral popliteal arterial reconstruction, J. Cardiovasc. Surg 8 (3) (1967) 195–197 (Torino).

[13]. de Vries MR, Simons KH, Jukema JW, Braun J, Quax PH, Vein graft failure: from pathophysiology to clinical outcomes, Nat. Rev. Cardiol. 13 (8) (2016) 451–470. [PubMed: 27194091]

[14]. Taggart DP, Current status of arterial grafts for coronary artery bypass grafting, Ann. Cardiothorac. Surg. 2 (4) (2013) 427–430. [PubMed: 23977618]

[15]. Tranbaugh RF, Schwann TA, Swistel DG, Dimitrova KR, Al-Shaar L, Hoffman DM, Geller CM, Engoren M, Balaram SK, Puskas JD, Habib RH, Coronary artery bypass graft surgery using the radial artery, right internal thoracic artery, or saphenous vein as the second conduit, Ann. Thorac. Surg. 104 (2) (2017) 553–559. [PubMed: 28215422]

[16]. McKavanagh P, Yanagawa B, Zawadowski G, Cheema A, Management and prevention of saphenous vein graft failure: a review, Cardiol. Ther. 6 (2) (2017) 203–223. [PubMed: 28748523]

[17]. Popovic B, Voillot D, Maureira P, Vanhuyse F, Agrinier N, Aliot E, Folliguet T, Villemot JP, Bilateral internal mammary artery bypass grafting: long-term clinical benefits in a series of 1000 patients, Heart 99 (12) (2013) 854–859. [PubMed: 23514978]

[18]. So SI, Coronary artery bypass surgery versus percutaneous coronary intervention with stent implantation in patients with multivessel coronary artery disease (the stent or surgery trial): a randomised controlled trial, Lancet 360 (9338) (2002) 965–970. [PubMed: 12383664]

[19]. Hillis LD, Smith PK, Anderson JL, Bittl JA, Bridges CR, Byrne JG, Cigarroa JE, Disesa VJ, Hiratzka LF, Hutter AM, Jessen ME, Keeley EC, Lahey SJ, Lange RA, London MJ, Mack MJ, Patel MR, Puskas JD, Sabik JF, Selnes O, Shahian DM, Trost JC, Winniford MD, F. American College of Cardiology, G. American Heart Association Task Force on Practice, S. American Association for Thoracic, A. Society of Cardiovascular, and S. Society of Thoracic, 2011 ACCF/AHA guideline for coronary artery bypass graft surgery. A report of the American College of cardiology foundation/American heart association task force on practice guidelines. Developed in collaboration with the American association for Thoracic surgery, society of cardiovascular anesthesiologists, and society of thoracic surgeons, J. Am. Coll. Cardiol. 58 (24) (2011) e123–e210. [PubMed: 22070836]

[20]. Rosales A, Valve reconstructions, Phlebology 30 (1 Suppl.) (2015) 50–58. [PubMed: 25729068]

[21]. Darwood RJ, Theivacumar N, Dellagrammaticas D, Mavor AI, Gough MJ, Randomized clinical trial comparing endovenous laser ablation with surgery for the treatment of primary great saphenous varicose veins, Br. J. Surg. 95 (3) (2008) 294–301. [PubMed: 18278775]

[22]. Merchant RF, Pichot O, Study GC, Long-term outcomes of endovenous radiofrequency obliteration of saphenous reflux as a treatment for superficial venous insufficiency, J. Vasc. Surg. 42 (3) (2005) 502–509 discussion 509. [PubMed: 16171596]

[23]. Dalsing MC, Lalka SG, Unthank JL, Grieshop RJ, Nixon C, Davis T, Venous valvular insufficiency: influence of a single venous valve (native and experimental), J. Vasc. Surg. 14 (5) (1991) 576–587. [PubMed: 1942365]

[24]. Kim YS, Majid M, Melchiorri AJ, Mikos AG, Applications of decellularized extracellular matrix in bone and cartilage tissue engineering, Bioeng. Trans. Med. 4 (1) (2019) 83–95.

[25]. Badylak SF, The extracellular matrix as a scaffold for tissue reconstruction, Semin. Cell Dev. Biol. 13 (5) (2002) 377–383. [PubMed: 12324220]

[26]. Bonnans C, Chou J, Werb Z, Remodelling the extracellular matrixin development and disease, Nat. Rev. Mol. Cell Biol. 15 (12) (2014) 786–801. [PubMed: 25415508]

[27]. Hynes RO, The extracellular matrix: not just pretty fibrils, Science 326 (5957) (2009) 1216–1219. [PubMed: 19965464]

[28]. Du J, Chen X, Liang X, Zhang G, Xu J, He L, Zhan Q, Feng XQ, Chien S, Yang C, Integrin activation and internalization on soft ECM as a mechanism of induction of stem cell differentiation by ECM elasticity, Proc. Natl. Acad. Sci. U S A 108 (23) (2011) 9466–9471. [PubMed: 21593411]

[29]. Huleihel L, Dziki JL, Bartolacci JG, Rausch T, Scarritt ME, Cramer MC, Vorobyov T, LoPresti ST, Swineheart IT, White LJ, Brown BN, Badylak SF, Macrophage phenotype in response to ECM bioscaffolds, Semin. Immunol. 29 (2017) 2–13. [PubMed: 28736160]

[30]. Barker TH, The role of ECM proteins and protein fragments in guiding cell behavior in regenerative medicine, Biomaterials 32 (18) (2011) 4211–4214. [PubMed: 21515169]

[31]. Borghi N, Lowndes M, Maruthamuthu V, Gardel ML, Nelson WJ, Regulation of cell motile behavior by crosstalk between cadherin- and integrin-mediated adhesions, Proc. Natl. Acad. Sci. USA 107 (30) (2010) 13324–13329. [PubMed: 20566866]

[32]. Lukashev ME, Werb Z, ECM signalling: orchestrating cell behaviour and misbehaviour, Trends Cell Biol. 8 (11) (1998) 437–441. [PubMed: 9854310]

[33]. Ingber D, Extracellular matrix and cell shape: potential control points for inhibition of angiogenesis, J. Cell. Biochem. 47 (3) (1991) 236–241. [PubMed: 1724246]

[34]. Abbott WM, Megerman J, Hasson JE, L'Italien G, Warnock DF, Effect of compliance mismatch on vascular graft patency, J. Vasc. Surg. 5 (2) (1987) 376–382. [PubMed: 3102762]

[35]. Mancuso L, Gualerzi A, Boschetti F, Loy F, Cao G, Decellularized ovine arteries assmall-diameter vascular grafts, Biomed. Mater. 9 (4) (2014) 045011. [PubMed: 25050540]

[36]. Crapo PM, Gilbert TW, Badylak SF, An overview of tissue and whole organ decellularization processes, Biomaterials 32 (12) (2011) 3233–3243. [PubMed: 21296410]

[37]. Schaner PJ, Martin ND, Tulenko TN, Shapiro IM, Tarola NA, Leichter RF, Carabasi RA, Dimuzio PJ, Decellularized vein as a potential scaffold for vascular tissue engineering, J. Vasc. Surg. 40 (1) (2004) 146–153. [PubMed: 15218475]

[38]. Bertanha M, Moroz A, Jaldin RG, Silva RA, Rinaldi JC, Golim MA,Felisbino SL, Domingues MA, Sobreira ML, Reis PP, Deffune E, Morphofunctional characterization of decellularized vena cava as tissue engineering scaffolds, Exp. Cell Res. 326 (1) (2014) 103–111. [PubMed: 24929113]

[39]. Simsa R, Padma AM, Heher P, Hellstrom M, Teuschl A, Jenndahl L, Bergh N, Fogelstrand P, Systematic in vitro comparison of decellularization protocols for blood vessels, PLoS ONE 13 (12) (2018) e0209269. [PubMed: 30557395]

[40]. Lemson MS, Tordoir JH, Daemen MJ, Kitslaar PJ, Intimal hyperplasia in vascular grafts, Eur. J. Vasc. Endovasc. Surg. 19 (4) (2000) 336–350. [PubMed: 10801366]

[41]. Human P, Zilla P, Inflammatory and immune processes: the neglected villain of bioprosthetic degeneration? J. Long Term Eff. Med. Implants 11 (3–4) (2001) 199–220. [PubMed: 11921664]

[42]. Quint C, Kondo Y, Manson RJ, Lawson JH, Dardik A, Niklason LE, Decellularized tissue-engineered blood vessel as an arterial conduit, Proc. Natl. Acad. Sci. U S A 108 (22) (2011) 9214–9219. [PubMed: 21571635]

[43]. Sharp MA, Phillips D, Roberts I, Hands L, A cautionary case: the synergraft vascular prosthesis, Eur. J. Vasc. Endovasc. Surg. 27 (1) (2004) 42–44. [PubMed: 14652835]

[44]. Lehr EJ, Rayat GR, Chiu B, Churchill T, McGann LE, Coe JY, Ross DB, Decellularization reduces immunogenicity of sheep pulmonary artery vascular patches, J. Thorac. Cardiovasc. Surg. 141 (4) (2011) 1056–1062. [PubMed: 20637475]

[45]. Zou Y, Zhang Y, Mechanical evaluation of decellularized porcine thoracic aorta, J. Surg. Res. 175 (2) (2012) 359–368. [PubMed: 21571306]

[46]. Tepekoylu C, Lobenwein D, Blunder S, Kozaryn R, Dietl M, Ritschl P, Pechriggl EJ, Blumer MJ, Bitsche M, Schistek R, Kotsch K, Fritsch H, Grimm M, Holfeld J, Alteration of inflammatory response by shock wave therapy leads to reduced calcification of decellularized aortic xenografts in micedagger, Eur. J. Cardiothorac. Surg 47 (3) (2015) e80–e90. [PubMed: 25422292]

[47]. Sheridan WS, Duffy GP, Murphy BP, Mechanical characterization of a customized decellularized scaffold for vascular tissue engineering, J. Mech. Behav. Biomed. Mater. 8 (2012) 58–70. [PubMed: 22402154]

[48]. Lin CH, Kao YC, Lin YH, Ma H, Tsay RY, A fiber-progressive-engagement model to evaluate the composition, microstructure, and nonlinear pseudoelastic behavior of porcine arteries and decellularized derivatives, Acta Biomater. 46 (2016) 101–111. [PubMed: 27667016]

[49]. Liu ZZ, Wong ML, Griffiths LG, Effect of bovine pericardial extracellular matrix scaffold niche on seeded human mesenchymal stem cell function, Sci. Rep. 6 (2016) 37089. [PubMed: 27845391]

[50]. Dalgliesh AJ, Parvizi M, Lopera-Higuita M, Shklover J, Griffiths LG, Graft-specific immune tolerance is determined by residual antigenicity of xenogeneic extracellular matrix scaffolds, Acta Biomater. 79 (2018) 253–264. [PubMed: 30130615]

[51]. Gates KV, Pereira NL, Griffiths LG, Cardiac non-human leukocyte antigen identification: techniques and troubles, Front. Immunol. 8 (2017) 1332. [PubMed: 29093713]

[52]. Griffiths LG, Choe LH, Reardon KF, Dow SW, COrton E, Immunoproteomic identification of bovine pericardium xenoantigens, Biomaterials 29 (26) (2008) 3514–3520. [PubMed: 18514307]

[53]. Deiwick M, Glasmacher B, Baba HA, Roeder N, Reul H,Von Bally G, Scheld HH, In vitro *testing of bioprostheses: influence of mechanical stresses and lipids on calcification*, Ann. Thorac. Surg. 66 (6 Suppl.) (1998) S206–S211. [PubMed: 9930449]

[54]. Van Nooten G, Somers P, Cornelissen M, Bouchez S, Gasthuys F, Cox E, Sparks L, Narine K, Acellular porcine and kangaroo aortic valve scaffolds show more intense immune-mediated calcification than cross-linked toronto SPV valves in the sheep model, Interact. Cardiovasc. Thorac. Surg. 5 (5) (2006) 544–549. [PubMed: 17670642]

[55]. Konakci KZ, Bohle B, Blumer R, Hoetzenecker W, Roth G, Moser B, Boltz-Nitulescu G, Gorlitzer M, Klepetko W, Wolner E, Ankersmit HJ, Alpha-gal on bioprostheses: xenograft immune response in cardiac surgery, Eur. J. Clin. Invest. 35 (1) (2005) 17–23. [PubMed: 15638815]

[56]. Keane TJ, Londono R, Turner NJ, Badylak SF, Consequences of ineffective decellularization of biologic scaffolds on the host response, Biomaterials 33 (6) (2012) 1771–1781. [PubMed: 22137126]

[57]. Dall'Olmo L, Zanusso I, Di Liddo R, Chioato T, Bertalot T, Guidi E, Conconi MT, Blood vessel-derived acellular matrix for vascular graft application, Biomed. Res. Int. 2014 (2014) 685426. [PubMed: 25136610]

[58]. Mehigan DG, Fitzpatrick B, Browne HI, Bouchier-Hayes DJ, Is compliance mismatch the major cause of anastomotic arterial aneurysms? Analysis of 42 cases, J. Cardiovasc. Surg. 26 (2) (1985) 147–150 (Torino).

[59]. Alfonso-Garcia A, Shklover J, Sherlock BE, Panitch A, Griffiths LG, Marcu L, Fiber-based fluorescence lifetime imaging of recellularization processes on vascular tissue constructs, J. Biophotonics 11 (9) (2018) e201700391. [PubMed: 29781171]

[60]. Lopera Higuita M, Griffiths LG, Small diameter xenogeneic extracellular matrix scaffolds f or vascular applications, Tissue Eng. Part B Rev. 26 (1) (2020) 26–45. [PubMed: 31663438]

[61]. Papalamprou A, Griffiths LG, Cardiac extracellular matrix scaffold generated using sarcomeric disassembly and antigen removal, Ann. Biomed. Eng. 44 (4) (2016) 1047–1060. [PubMed: 26215309]

[62]. Lopera Higuita M, Griffiths LG, Antigen removal process preserves function of small diameter venous valved conduits, whereas SDS-decellularization results in significant valvular insufficiency, Acta Biomater. (2020).

[63]. Baer MT, Huang N, Gibson FC 3rd, scavenger receptor A is expressed by macrophages in response to porphyromonas gingivalis, and participates in TNF-alpha expression, Oral Microbiol. Immunol. 24 (6) (2009) 456–463. [PubMed: 19832797]

[64]. Wong ML, Wong JL, Athanasiou KA, Griffiths LG, Stepwise solubilization-based antigen removal for xenogeneic scaffold generation in tissue engineering, Acta Biomater. 9 (5) (2013) 6492–6501. [PubMed: 23321301]

[65]. Wong ML, Leach JK, Athanasiou KA, Griffiths LG, The role of protein solubilization in antigen removal from xenogeneic tissue for heart valve tissue engineering, Biomaterials 32 (32) (2011) 8129–8138. [PubMed: 21810537]

[66]. Wong ML, Wong JL, Vapniarsky N, Griffiths LG, In vivo xenogeneics caffold fate is determined by residual antigenicity and extracellular matrix preservation, Biomaterials 92 (2016) 1–12. [PubMed: 27031928]

[67]. Badylak SF, Gilbert TW, Immune response to biologic scaffold materials, Semin. Immunol. 20 (2) (2008) 109–116. [PubMed: 18083531]

[68]. Fishman JM, Lowdell MW, Urbani L, Ansari T, Burns AJ, Turmaine M, North J, Sibbons P, Seifalian AM, Wood KJ, Birchall MA, De Coppi P, Immunomodulatory effect of a decellularized skeletal muscle scaffold in a discordant xenotransplantation model, Proc. Natl. Acad. Sci. U S A 110 (35) (2013) 14360–14365. [PubMed: 23940349]

[69]. Allaire E, Bruneval P, Mandet C, Becquemin JP, Michel JB, The immunogenicity of the extracellular matrix in arterial xenografts, Surgery 122 (1) (1997) 73–81. [PubMed: 9225918]

[70]. DeLustro F, Dasch J, Keefe J, Ellingsworth L, Immune responses to allogeneic and xenogeneic implants of collagen and collagen derivatives, Clin. Orthop. Relat. Res. (260) (1990) 263–279.

[71]. Bayrak A, Tyralla M, Ladhoff J, Schleicher M, Stock UA, Volk HD, Seifert M, Human immune responses to porcine xenogeneic matrices and their extracellular matrix constituents in vitro, Biomaterials 31 (14) (2010) 3793–3803. [PubMed: 20171732]

[72]. Rieder E, Nigisch A, Dekan B, Kasimir MT, Muhlbacher F, Wolner E, Simon P, Weigel G, Granulocyte-based immune response against decellularized or glutaraldehyde cross-linked vascular tissue, Biomaterials 27 (33) (2006) 5634–5642. [PubMed: 16889827]

[73]. Xiong Y, Chan WY, Chua AW, Feng J, Gopal P, Ong YS, Song C, Decellularized porcine saphenous artery for small-diameter tissue-engineered conduit graft, Artif. Organs 37 (6) (2013) E74–E87. [PubMed: 23566255]

[74]. Liu GF, He ZJ, Yang DP, Han XF, Guo TF, Hao CG, Ma H, Nie CL, Decellularized aorta of fetal pigs as a potential scaffold for small diameter tissue engineered vascular graft, Chin. Med. J. 121 (15) (2008) 1398–1406 (Engl.). [PubMed: 18959117]

[75]. Morris AH, Stamer DK, Kyriakides TR, The host response to naturally-derived extracellular matrix biomaterials, Semin. Immunol. 29 (2017) 72–91. [PubMed: 28274693]

[76]. Aller MA, Arias JL, Nava MP, Arias J, Posttraumatic inflammation is a complex response based on the pathological expression of the nervous, immune, and endocrine functional systems, Exp. Biol. Med. 229 (2) (2004) 170–181 (Maywood).

[77]. María Ángeles Aller LL, Arias JL, Fabián GR, Alonso MS, Begega A, López L, Gómez JR, Arias J, Thepsycho-neuro-immune-endocrine response: a physiological and pathological way of life, Psicothema 8 (2) (1996).

[78]. Aller MA, Arias JL, Lorente L, Nava MP, Duran HJ, Arias J, Neuro-immune-endocrine functional system and vascular pathology, Med. Hypotheses 57 (5) (2001) 561–569. [PubMed: 11735311]

[79]. Davies PF, Tripathi SC, Mechanical stress mechanisms and the cell. An endothelial paradigm, Circ. Res. 72 (2) (1993) 239–245. [PubMed: 8418981]

[80]. Aller MA, Arias JL, Sanchez-Patan F, Arias J, The inflammatory response: an efficient way of life, Med. Sci. Monit. 12 (10) (2006) RA225–34. [PubMed: 17006415]

[81]. Luan NM, Iwata H, Long-term allogeneic islet graft survival in prevascularized subcutaneous sites without immunosuppressive treatment, Am. J. Transplant. 14 (7) (2014) 1533–1542. [PubMed: 24909185]

[82]. Al-Soudi A, Kaaij MH, Tas SW, Endothelial cells: from innocent bystanders to active participants in immune responses, Autoimmun. Rev. 16 (9) (2017) 951–962. [PubMed: 28698091]

[83]. Kumar H, Kawai T, Akira S, Pathogen recognition by the innate immune system, Int. Rev. Immunol. 30 (1) (2011) 16–34. [PubMed: 21235323]

[84]. Davis GE, Bayless KJ, Davis MJ, Meininger GA, Regulation of tissue injury responses by the exposure of matricryptic sites within extracellular matrix molecules, Am. J. Pathol. 156 (5) (2000) 1489–1498. [PubMed: 10793060]

[85]. Adair-Kirk TL, Senior RM, Fragments of extracellular matrix as mediators of inflammation, Int. J. Biochem. Cell Biol. 40 (6–7) (2008) 1101–1110. [PubMed: 18243041]

[86]. Medzhitov R, Janeway C Jr., Innate immune recognition: mechanisms and pathways, Immunol. Rev. 173 (2000) 89–97. [PubMed: 10719670]

[87]. Davis GE, Matricryptic sites control tissue injury responses in the cardiovascular system: relationships to pattern recognition receptor regulated events, J. Mol. Cell Cardiol. 48 (3) (2010) 454–460. [PubMed: 19751741]

[88]. Gilbert TW, Sellaro TL, Badylak SF, Decellularization of tissues and organs, Biomaterials 27 (19) (2006) 3675–3683. [PubMed: 16519932]

[89]. Gilpin SE, Guyette JP, Gonzalez G, Ren X, Asara JM, Mathisen DJ, Vacanti JP, Ott HC, Perfusion decellularization of human and porcine lungs: bringing the matrix to clinical scale, J. Heart Lung Transplant. 33 (3) (2014) 298–308. [PubMed: 24365767]

[90]. Korossis SA, Booth C, Wilcox HE, Watterson KG, Kearney JN, Fisher J, Ingham E, Tissue engineering of cardiac valve prostheses II: biomechanical characterization of decellularized porcine aortic heart valves, J. Heart Valve Dis. 11 (4) (2002) 463–471. [PubMed: 12150291]

[91]. Ott HC, Matthiesen TS, Goh SK, Black LD, Kren SM, Netoff TI, Taylor DA, Perfusion-decellularized matrix: using nature's platform to engineer a bioartificial heart, Nat. Med. 14 (2) (2008) 213–221. [PubMed: 18193059]

[92]. Faulk DM, Carruthers CA, Warner HJ, Kramer CR, Reing JE, Zhang L, D'Amore A, Badylak SF, The effect of detergents on the basement membrane complex of a biologic scaffold material, Acta Biomater. 10 (1) (2014) 183–193. [PubMed: 24055455]

[93]. Hwang J, San BH, Turner NJ, White LJ, Faulk DM, Badylak SF, Li Y, Yu SM, Molecular assessment of collagen denaturation in decellularizedtissues using a collagen hybridizing peptide, Acta Biomater. 53 (2017) 268–278. [PubMed: 28161576]

[94]. Gowen BB, Borg TK, Ghaffar A, Mayer EP, Selective adhesion of macrophages to denatured forms of type I collagen is mediated by scavenger receptors, Matrix Biol. 19 (1) (2000) 61–71. [PubMed: 10686426]

[95]. El Khoury J, Thomas CA, Loike JD, Hickman SE, Cao L, Silverstein SC, Macrophages adhere to glucose-modified basement membrane collagen IV via their scavenger receptors, J. Biol. Chem. 269 (14) (1994) 10197–10200. [PubMed: 8144597]

[96]. Anderson JM, Rodriguez A, Chang DT, Foreign body reaction to biomaterials, Semin. Immunol. 20 (2) (2008) 86–100. [PubMed: 18162407]

[97]. Allaire E, Guettier C, Bruneval P, Plissonnier D, Michel JB, Cell-free arterial grafts: morphologic characteristics of aortic isografts, allografts, and xenografts in rats, J. Vasc. Surg. 19 (3) (1994) 446–456. [PubMed: 8126857]

[98]. Knapp J, Rizzo A, Maxwell M, Duran C, Cheung D, Evaluation of a bovine vascular graft in sheep, Mil. Med. 181 (5 Suppl.) (2016) 240–246. [PubMed: 27168579]

[99]. Orenstein SB, Saberski ER, Kreutzer DL, Novitsky YW, Comparative analysis of histopathologic effects of synthetic meshes based on material, weight, and pore size in mice, J. Surg. Res. 176 (2) (2012) 423–429. [PubMed: 22099590]

[100]. Junge K, Binnebosel M, von Trotha KT, Rosch R, Klinge U, Neumann UP, Lynen Jansen P, Mesh biocompatibility: effects of cellular inflammation and tissue remodelling, Langenbecks Arch. Surg. 397 (2) (2012) 255–270. [PubMed: 21455703]

[101]. Ruffer A, Purbojo A, Cicha I, Glockler M, Potapov S, Dittrich S, Cesnjevar RA, Early failure of xenogenous de-cellularised pulmonary valve conduits–a word of caution!, Eur. J. Cardiothorac. Surg. 38 (1) (2010) 78–85. [PubMed: 20219384]

[102]. Boer U, Spengler C, Jonigk D, Klingenberg M, Schrimpf C, Lutzner S, Harder M, Kreipe HH, Haverich A, Wilhelmi M, Coating decellularized equine carotid arteries with CCN1 improves cellular repopulation, local biocompatibility, and immune response in sheep, Tissue Eng. Part A 19 (15–16) (2013) 1829–1842. [PubMed: 23521030]

[103]. Boer U, Lohrenz A, Klingenberg M, Pich A, Haverich A, Wilhelmi M, The effect of detergent-based decellularization procedures on cellular proteins and immunogenicity in equine carotid artery grafts, Biomaterials 32 (36) (2011) 9730–9737. [PubMed: 21944468]

[104]. Faulk DM, Johnson SA, Zhang L, Badylak SF, Role of the extracellular matrix in whole organ engineering, J. Cell. Physiol. 229 (8) (2014) 984–989. [PubMed: 24347365]

[105]. Herbst TJ, McCarthy JB, Tsilibary EC, Furcht LT, Differential effects of laminin, intact type IV collagen, and specific domains of type IV collagen on endothelial cell adhesion and migration, J. Cell Biol. 106 (4) (1988) 1365–1373. [PubMed: 3360855]

[106]. Kubota Y, Kleinman HK, Martin GR, Lawley TJ, Role of laminin and basement membrane in the morphological differentiation of human endothelial cells into capillary-like structures, J. Cell Biol. 107 (4) (1988) 1589–1598. [PubMed: 3049626]

[107]. Madri JA, Pratt BM, Yannariello-Brown J, Matrix-driven cell size change modulates aortic endothelial cell proliferation and sheet migration, Am. J. Pathol. 132 (1) (1988) 18–27. [PubMed: 3394798]

[108]. Tilling T, Engelbertz C, Decker S, Korte D, Huwel S, Galla HJ, Expression and adhesive properties of basement membrane proteins in cerebral capillary endothelial cell cultures, Cell Tissue Res. 310 (1) (2002) 19–29. [PubMed: 12242480]

[109]. Teebken OE, Haverich A, Tissue engineering of small diameter vascular grafts, Eur. J. Vasc. Endovasc. Surg. 23 (6) (2002) 475–485. [PubMed: 12093061]

[110]. Conklin BS, Richter ER, Kreutziger KL, Zhong DS, Chen C, Development and evaluation of a novel decellularized vascular xenograft, Med. Eng. Phys. 24 (3) (2002) 173–183. [PubMed: 12062176]

[111]. Ma X, He Z, Li L, Liu G, Li Q, Yang D, Zhang Y, Li N, Development and in vivo validation of tissue-engineered, small-diameter vascular grafts from decellularized aortae of fetal pigs and canine vascular endothelial cells, J. Cardiothorac. Surg. 12 (1) (2017) 101. [PubMed: 29178903]

[112]. Bai H, Wang Z, Li M, Sun P, Wang W, Liu W, Wei S, Wang Z, Xing Y, Dardik A, A rat arteriovenous graft model using decellularized vein, Vascular 28 (5) (2020) 664–672. [PubMed: 32390561]

[113]. Jiang B, Suen R, Wertheim JA, Ameer GA, Targeting heparin to collagen within extracellular matrix significantly reduces thrombogenicity and improves endothelialization of decellularized tissues, Biomacromolecules 17 (12) (2016) 3940–3948. [PubMed: 27936727]

[114]. Cines DB, Pollak ES, Buck CA, Loscalzo J, Zimmerman GA, McEver RP, Pober JS, Wick TM, Konkle BA, Schwartz BS, Barnathan ES, McCrae KR, Hug BA, Schmidt AM, Stern DM, Endothelial cells in physiology and in the pathophysiology of vascular disorders, Blood 91 (10) (1998) 3527–3561. [PubMed: 9572988]

Statement of significance

The use of autologous vessels for the treatment of small diameter vascular diseases is common practice. However, the use of autologous tissue poses significant complications due to tissue harvest and limited availability. Developing an alternative vessel for use for the treatment of small diameter vessel diseases can potentially increase the success rate of autologous vascular grafting by eliminating complications related to the use of autologous vessel and increased availability. This manuscript demonstrates the potential of non-antigenic extracellular matrix (ECM) scaffolds derived from xenogeneic vascular tissue as off-the-shelf vascular grafts for the treatment of small diameter vascular diseases.

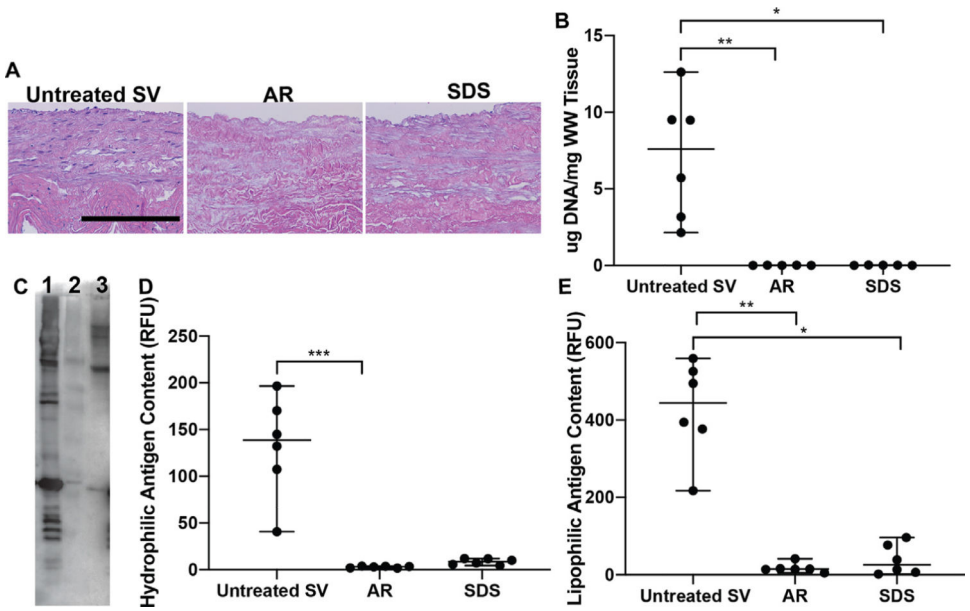

Fig. 1.

Cellularity and content of unknown minor histocompatibility antigens in saphenous vein ECM scaffolds. (A) Both AR and SDS-decellularization processing methods were successful at decellularizing SV scaffolds determined by the lack of visible nuclei. Scale bar 200 μm. (B) Similarly, both processing methods resulted in scaffolds with significantly low levels of DNA content compared to untreated SV. (C) Via western blot, AR (Lane-2) was capable of significantly reducing both hydrophilic (D) and lipophilic (E) unknown minor histocompatibility antigens when compared to untreated SV (Lane–1). SDS (Lane–3) decellularization also reduced both hydrophilic and lipophilic antigens, however only lipophilic reduction was statistically different from untreated SV. Lack of statistical significance of hydrophilic antigen reduction for SDS scaffolds may be related to the nature of the non-parametric statistical tests utilized (Wilcoxon/Kruskal-Wallis Test with Dunn *post-hoc* analysis on non-parametric medians). * = p <0.05, ** = p < 0.01, *** = p < 0.001.

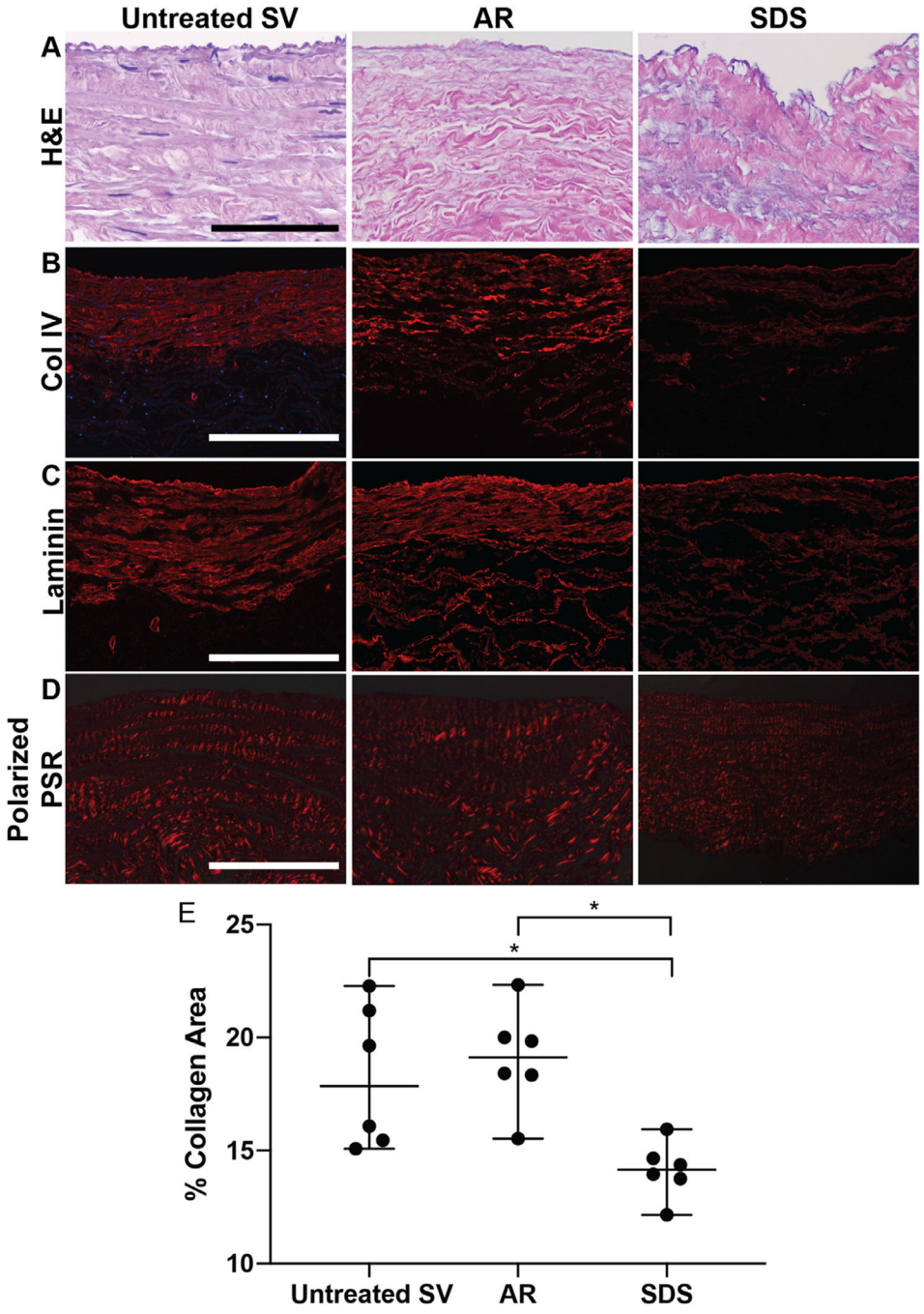

Fig. 2.

Macromolecular structure and retention of basement membrane integrity in SV ECM scaffolds. (A) AR preserved SV collagen organization (scale bar 100 μm), collagen IV (B, scale bar 200 μm) and laminin (C, scale bar 200 μm) content and organization, when compared to untreated SV. (A) Conversely, SDS-decellularization resulted in the disruption of abluminal collagen organization and a decrease in collagen IV (B) and laminin (C) content. (D, E, scale bar 200 μm). Similarly, AR retained the collagen alignment of

untreated SV, while SDS scaffolds significantly decreased collagen alignment. Wilcoxon/Kruskal-Wallis Test with Dunn *post-hoc* analysis on non-parametric medians. * = $p < 0.05$.

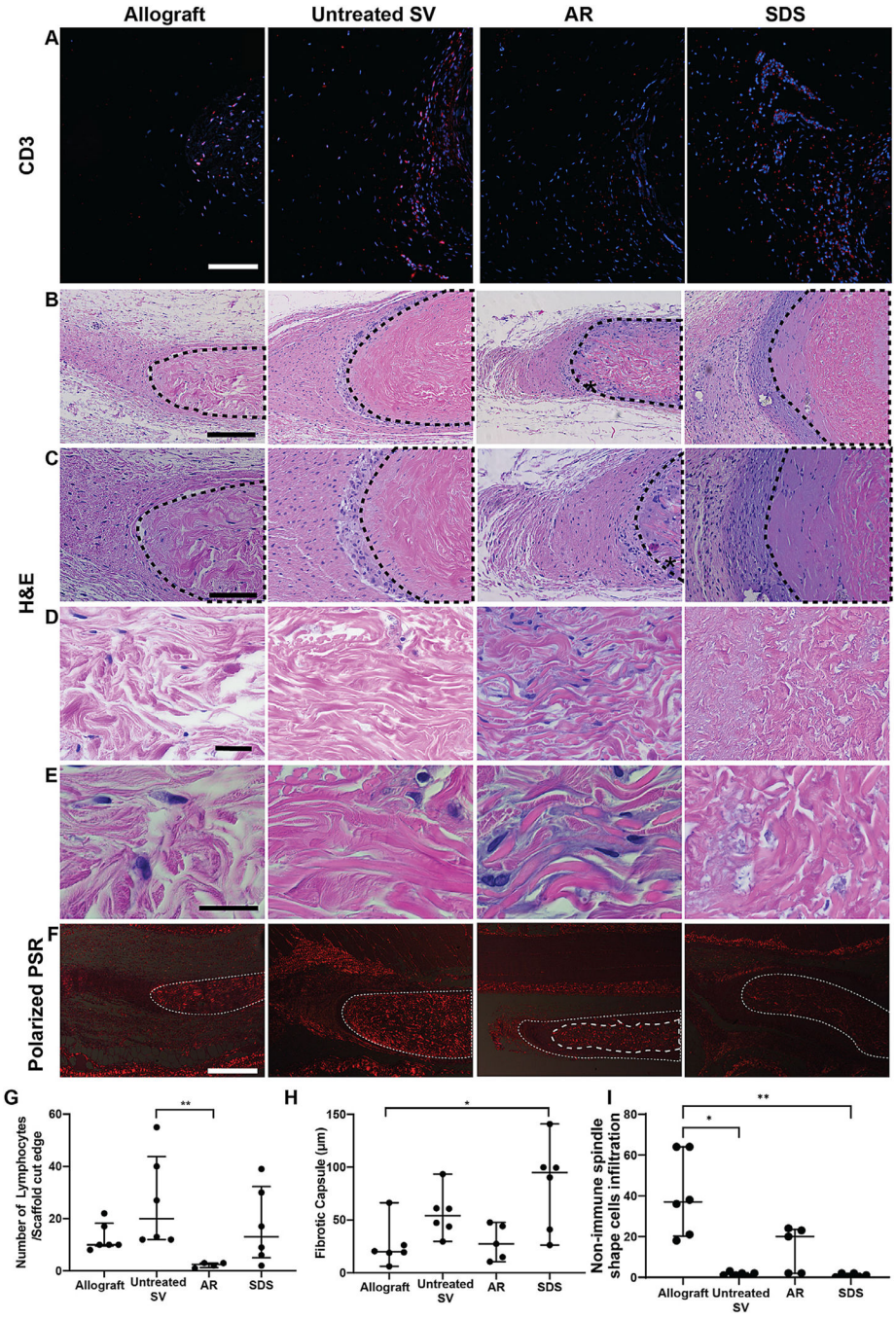

Fig. 3.

In vivo immune and pro-regenerative response towards subpannicularly implanted 1 × 1 cm scaffolds. Allografts implants were used as negative immunogenic controls. (A) Representative histological images of the cut edges of explanted scaffolds. Qualitatively, lymphocyte presence was comparable between AR and Allograft groups, whereas greater lymphocyte presence was identified in untreated or SDS SV scaffolds. (CD3 positive lymphocytes = red, DAPI stained nuclei = blue). Scale bar 100 μm.(B) H&E stained images demonstrate a higher number of non-lymphocytic, predominantly spindle shape cell

infiltration into AR-scaffold when compared to untreated SV and SDS-scaffolds (marked with an * in AR-scaffold, B, scale bar 200 μm. Dotted lines indicate location of scaffold), C (scale bar 100 μm), D (scale bar 50 μm), E (scale bar25μm). (F) Presence of these non-immune spindle shaped cells in AR scaffolds was associated with collagen reabsorption and scaffold turnover (newly formed collagen does not polarize-area within dashed lines in AR-scaffold) (Small dashed line represents original scaffold location (all groups), large dash line (AR group only) represents scaffoldcore which has yet to be turned over, continuing to polarize at pre-implantation levels). No evidence of scaffold turnover was seen in the other groups as evidenced by nochange in polarization compared to pre-implantation levels. Scale bar 500 μm. (G) Quantification of lymphocyte infiltration demonstrated that AR scaffolds significantly reduced graft-specific CD3 positive cell presence when compared to untreated SV. (H) The fibrotic encapsulation present in AR-scaffolds and untreated SV scaffolds was comparable to that of Allografts, while that found around the SDS-decellularized scaffolds was statistically higher than Allografts. (I) Quantification of infiltrating non-immunogenic spindle cells demonstrated AR scaffolds were not significantly different from allograft, whereas both untreated SV and SDS scaffolds had significantly lower cell infiltration. Wilcoxon/Kruskal-Wallis Test with Dunn *post-hoc* analysis on non-parametric medians. * = $p < 0.05$, ** = $p < 0.01$

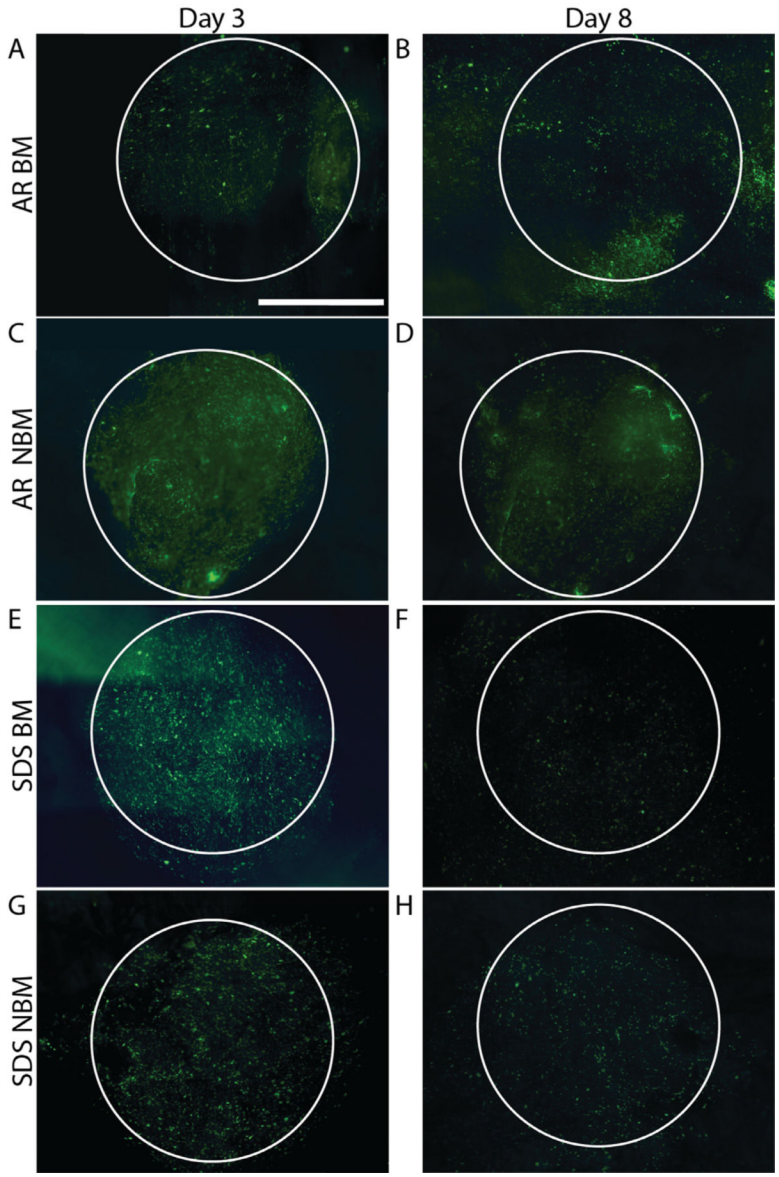

Fig. 4.

Recellularization capacity and cell modulatory capacity of SV ECM scaffolds. Both BM (A, B) and NBM (C,D) AR scaffolds ret ained their recellularization capacity determined by the presence of healthy endothelial cell layer at day 8 post seeding. Alternatively, the presence of endothelial cells in both BM (E, F) and NBM (G, H) SDS scaffolds was significantly diminished by day 8 post-seeding. Additionally, the presence of basement membrane proteins in AR BM (A, B) scaffolds modulated endothelial cells to spread more when compared to the cells on the other groups (original seeding shape demonstrate with white circle). Scale bar 2000 μm.

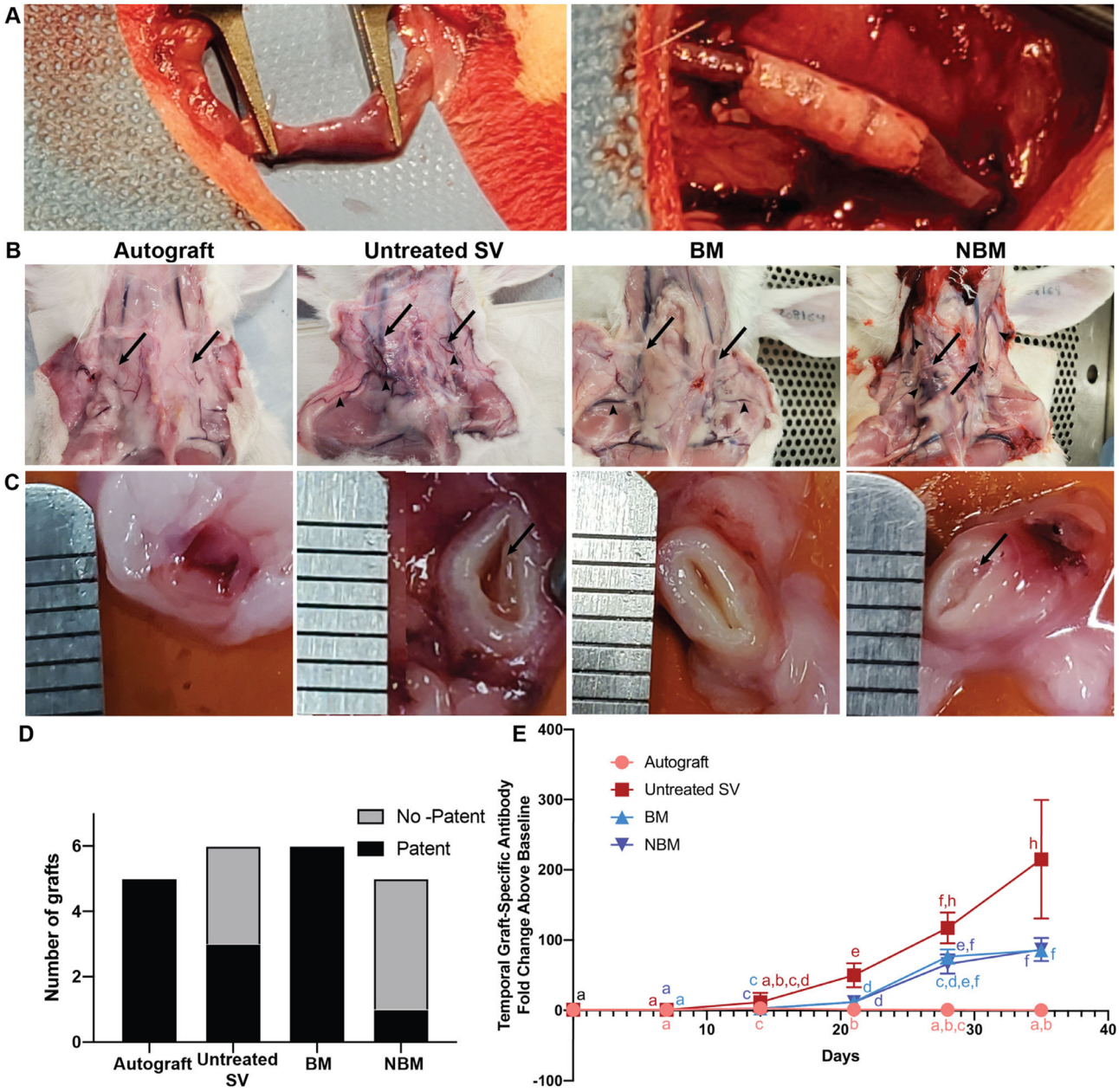

Fig. 5.

Gross pathology of *in vivo* jugular interposition grafts and associated humoral adaptive immune response. (A) Representative intraoperative surgical images of the jugular vein (left) and interposition graft (right) immediately after implantation. (B) Representative images of the interposition sites immediately before explantation (day 35), showing the graft location (arrows) and development of collateral vessels (arrow heads). (C) Representative cross-sectional image of the graft lumen in the mid-graft region for each group (ruler marks = 1 mm). Organized pre-mortem intraluminal thrombus is evident in the untreated SV and non-basement membrane groups (arrows), whereas the allograft and basement membrane groups have no evidence of thrombus formation. (D) Scaffolds in the Autograft and BM groups resulted in high patency rates, whereas untreated SV scaffolds and NBM scaffolds

resulted in low patency rates. (E) Graft specific antibody production towards all bovine scaffolds is first significantly different from autograft on day 21. Antibody production towards AR-scaffolds starts to plateau by day 28, while the antibody production towards untreated SV scaffolds continues to increase. Both AR groups stimulate significantly less graft-specific antibody production than that toward untreated SV scaffolds by day 35. Groups not connected by lower case letters are statistically different. Repeated measures two-way ANOVA and Tukey-Kramer HSD post-hoc analyses on standard least squares means.

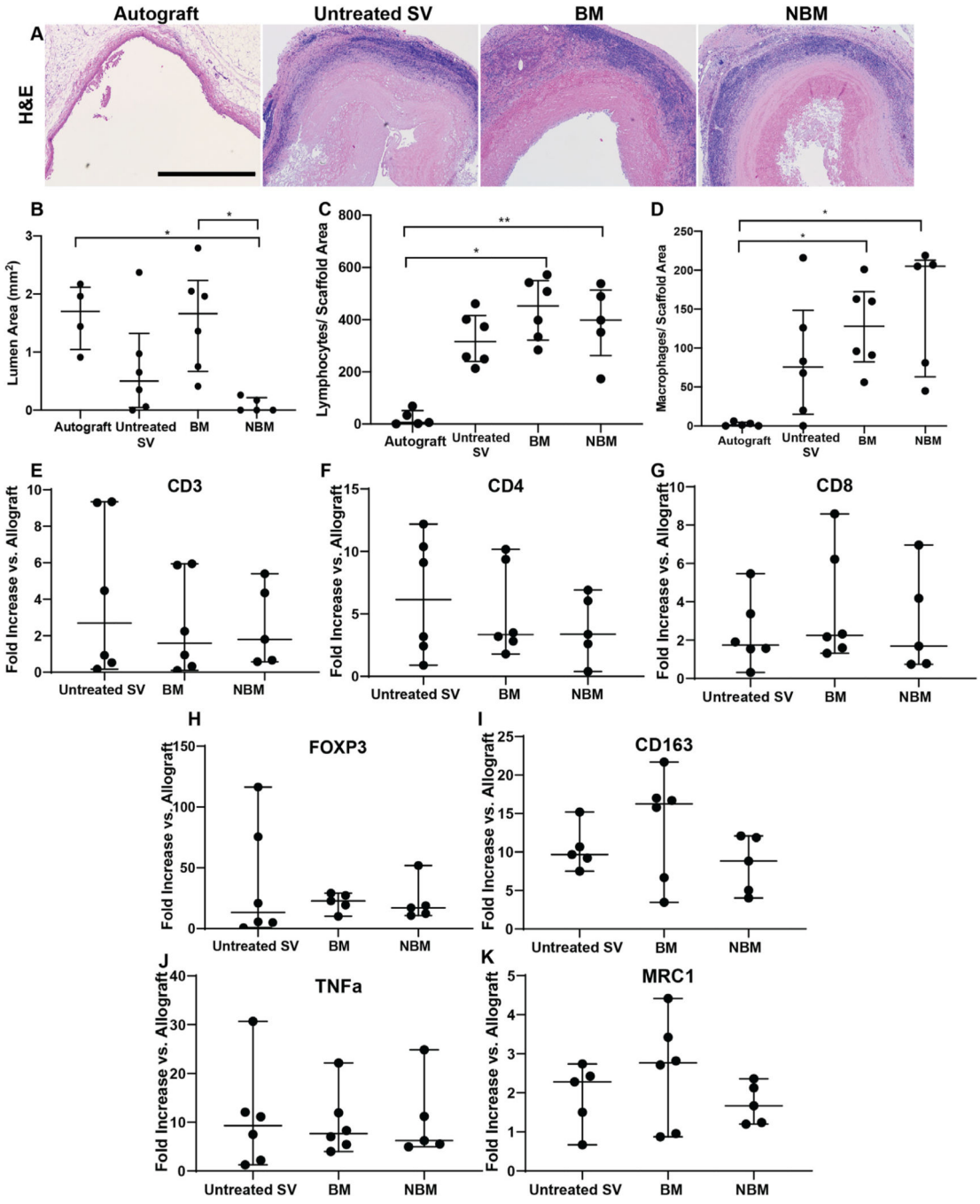

Fig. 6.

Rabbit *in vivo* response towards jugular interposition scaffolds. (A) All groups were evaluated for luminal area via histological assessment of H&E stained images. Scale bar 10 0 0 μm. (B) Presence of BM facing the vascular lumen maintains mid graft lumen area at levels equivalent to those of autograft. Conversely, absence of basement membrane components (NBM) resulted in significantly reduced mid-graft lumen area compared to basement membrane presence (BM) and Autograft groups. (C,D) Immune cell infiltration was assessed in all grafts via PCR. AR-scaffolds in both groups (BM

and NBM) resulted with significant lymphocyte (C) and macrophage infiltration (D)when compared to Autografts. No significant difference in the number of infiltrating lymphocytes or macrophages was identified between AR-scaffolds (BM and non-BM) and untreated SV tissue. (E–K) Subtype of lymphocytes and macrophages infiltrating the scaffolds was determined by real-time qPCR. CD3 (E), CD4 (F) and CD8 (G) genes were run to determine the amount of lymphocytes, while FOXP3 (H) was run to determine the presence of regulatory T cells (T_{reg}). Gene CD163 (I) was used to determine the total amount of macrophages, while TNF a (J) was used to determine M1 macrophage polarization and MRC1 (K) the presence of M2 polarized macrophages. Although no significant differences were found between groups for any of the immune cellular subtypes, definitive conclusions regarding the specific type of infiltrating immune cell could not be reached due to high data variability. * = $p < 0.05$, ** = $p < 0.01$.

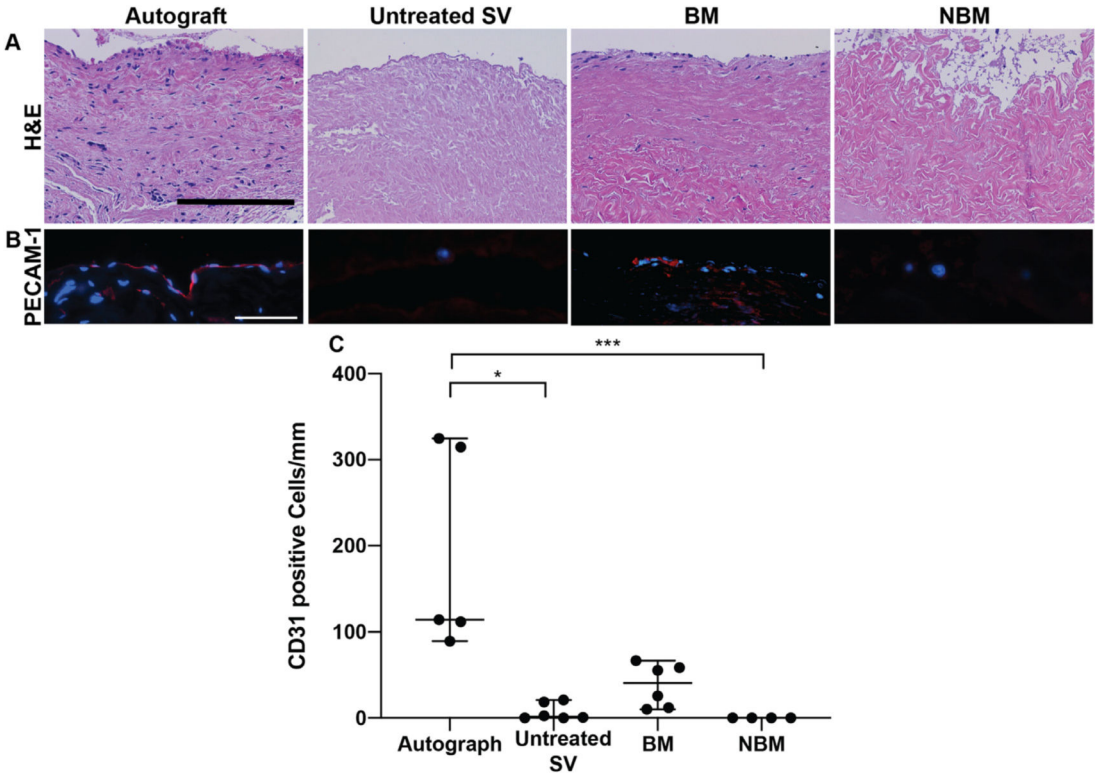

Fig. 7.

In vivo recellularization of scaffolds implanted in jugular interposition model. Scaffolds recellularization capability was determined by the degree of cell repopulation of scaffolds as seen in H&E histological images, platelet endothelial cell adhesion molecule (PECAM-1) staining and its quantification. (A) BM scaffolds experienced higher number of cell repopulation on the luminal surface and within the scaffold tunica media, whereas untreated SV scaffolds and NBM scaffolds resulted in very low overall cellular repopulation. It is possible some cell repopulation occurred in the Autograft scaffolds, however the majority of the cells were likely present before the surgical procedure. Scale bar 100 μm. (B) Positive PECAM-1 staining indicates some of the cells present in the luminal surface of BM scaffolds are endothelial cells. The difference in cells morphology and PECAM-1 secretion pattern of endothelial cell in the BM scaffolds from those in the Autograft scaffolds may be due to the short timeframe *in vivo* implantation. Scale bar 10 μm. (C) BM scaffolds experienced the highest number of endothelial cell repopulation in the lumen of the scaffold when compared to the other bovine groups. Due to the non-parametric statistics the number of endothelial cells found in the lumen of the BM scaffolds was not statistically different than that of the Autograft group although the absolute number is noticeably lower. Wilcoxon/Kruskal-Wallis Test with Dunn *post-hoc* analysis on non-parametric medians. * = $p < 0.05$, ** = $p < 0.01$, *** = $p < 0.001$.